Med Biol Eng Comput (2012) 50:773–799
DOI 10.1007/s11517-012-0924-6

REVIEW ARTICLE

Computational modeling of the human atrial anatomy and electrophysiology

Olaf Dössel · Martin W. Krueger · Frank M. Weber · Mathias Wilhelms · Gunnar Seemann

Received: 22 December 2011 / Accepted: 21 May 2012 / Published online: 21 June 2012

Abstract This review article gives a comprehensive survey of the progress made in computational modeling of the human atria during the last 10 years. Modeling the anatomy has emerged from simple "peanut"-like structures to very detailed models including atrial wall and fiber direction. Electrophysiological models started with just two cellular models in 1998. Today, five models exist considering e.g. details of intracellular compartments and atrial heterogeneity. On the pathological side, modeling atrial remodeling and fibrotic tissue are the other important aspects. The bridge to data that are measured in the catheter laboratory and on the body surface (ECG) is under construction. Every measurement can be used either for model personalization or for validation. Potential clinical applications are briefly outlined and future research perspectives are suggested.

Keywords Cardiac modeling · Atrial arrhythmia · Radio frequency ablation · Remodeling · Intraatrial electrograms

Abbreviations

AF	Atrial fibrillation
AP	Action potential
APD	Action potential duration
BB	Bachmann's bundle
BCL	Basic cycle length
BSP(M)	Body surface potential (map)
CS	Coronary sinus
CT	Crista terminalis
CT	Computed tomography
CV	Conduction velocity
ECG	Electrocardiogram
EP	Electrophysiology
ERP	Effective refractory period
IVC	Inferior vena cava
LA	Left atrium
LAA	Left atrial appendage
LIPV	Left inferior pulmonary vein
LE-MRI	Late enhancement MRI
LSPV	Left superior pulmonary vein
MRI	Magnetic resonance imaging
PM	Pectinate muscle
PV	Pulmonary vein
PWd	P-wave duration
RA	Right atrium
RAA	Right atrial appendage
RF(A)	Radio frequency (ablation)
RIPV	Right inferior pulmonary vein
RSPV	Right superior pulmonary vein
SN	Sinus node
SVC	Superior vena cava
TEE	Transesophageal echocardiogram
WL	Wave length

O. Dössel (✉) · M. W. Krueger · F. M. Weber · M. Wilhelms · G. Seemann
Institute of Biomedical Engineering, Karlsruhe Institute of Technology, Kaiserstr. 12, 76131 Karlsruhe, Germany
e-mail: olaf.doessel@kit.edu

F. M. Weber
Digital Imaging Department, Philips Research Laboratories, 22335 Hamburg, Germany

1 Introduction

Intensive research is carried out in the field of atrial physiology and pathophysiology, and both efforts and comprehension are increasing rapidly [215]. One

motivation for this endeavour lies in the fact that around 1 % of the population suffer from atrial fibrillation (AF). The incidence of AF increases significantly with age, that is why this topic is of utmost relevance in countries with aging population [215]. Since the year 2000, about 25 articles on comprehensive mathematical 3D-models of the atria and their electrophysiology and another 200 articles of various aspects on atrial modeling have been published. This strong research is motivated by the fact that computational modeling of the atria can contribute significantly to better comprehension of atrial physiology and pathophysiology. By that, it can lead to a more detailed diagnosis and improved therapy for millions of patients. Computational modeling enables a much deeper interpretation of experimental data and motivates new clinical research. We also find several review articles and book chapters on in silico modeling of the heart [29, 118, 166, 225, 239] and in particular the atria [97, 246]. The focus of this review article is 100 % on the atria and it will investigate the complete chain from the ion channels, the anatomy and the electrophysiology to the atrial intracardiac electrogram and the electrocardiogram (ECG). The review will demonstrate how simple models have evolved to sophisticated models that take into account heterogeneity of the atrial cells, details of the geometry and muscle strands, fiber direction and anisotropy, restitution curves, remodeling, fibrotic tissue and ablation scars. We will also try to bridge the gap between computational models and real measurements that are carried out every day in the electrophysiological laboratory (EP-lab) in the hospital.

2 Modeling the geometry of the atria

There is a strong link between the anatomy of the atria and the physiological excitation sequence. Also the onset and perpetuation of AF is connected to the anatomy [13, 85, 87, 90, 132]. Therefore, the following section briefly introduces gross atrial anatomy and focuses on the anatomical features relevant to atrial modeling. Comprehensive reviews about atrial anatomy can be found elsewhere [84, 85, 87].

2.1 Anatomy of the atria

The right atrium (RA) collects venous blood from the two caval veins and the coronary sinus (CS). The RA myocardium is separated into a smooth venous part and a rough free wall [87] by the crista terminalis (CT) [205]. The RA hosts the sinus node (SN), which is located at the junction of the superior caval vein (SVC) and the right atrial appendage (RAA) [206]. The triangular RAA clasps the aortic arch [205].

Usually, four pulmonary veins (PVs) connect to the left atrium (LA), which has a smooth endocardial surface. The posterior wall of the left atrium is close to the oesophagus [207]. The left atrial appendage (LAA) is clearly delineated and has a tubular shape with multiple finger-like branches [228]. The LA has a diameter of 3.7 cm [183, 240] and a volume of 42 ml in normal hearts [183]. An increase in left atrial volume is commonly linked to AF in clinical practice [214]. Atrial dilatation is therefore also subject to modeling studies (e.g. [198]).

The atria are connected via multiple interatrial bridges with Bachmann's bundle (BB) as the most prominent one, running from the area of the SN towards the LAA [88], bridging the interatrial grove [130, 248]. There is a high variability of the interatrial bundles between individuals [3, 88, 203].

2.1.1 Wall thickness

The wall of the human atria has a reported thickness between 1 and 3 mm [30, 40, 77, 165, 174, 180, 207, 229, 253]. Wall thickness in the RA is non-uniform due to the CT and pectinate muscles (PMs) [253]. The LA wall is thicker on the posterior and inferior side compared to the LA roof [77, 180]. Wang et al. [253] measured a thicker wall in the LA compared to the RA, whereas Neher et al. [165] reported the opposite (3.3 vs. 2.1 mm). Males have a slightly thicker atrial wall compared to females [77] and patients with AF often have a thinner left atrial wall (2.1–2.5 mm vs. 2.3–2.9 mm) [180]. The transmurality of a lesion made with radio frequency (RF) ablation depends on the regional varying atrial wall thickness [40, 174] or vice-versa the wall thickness has an impact on the energy needed to create a transmural lesion [18, 88].

2.1.2 Pulmonary veins

Paroxysmal AF is most often triggered by ectopic activity in the PVs [75]. The ostia of the PVs are therefore of increasing interest for the electrophysiologist and are also subject of simulation studies (e.g. [260, 237]). The diameter of the PV ostia is larger in the superior veins than in the inferior veins (11 vs. 8 mm) and is often increased in patients with AF triggered by ectopic foci in the PVs [137]. The wall of the PVs is around 0.5 mm thick [81].

Typically, four PVs from the five lung lobes connect to the LA (two left, two right) [21]. The vein from the right middle lung lobe thereby usually joins the upper lobe vein before reaching the LA [241]. Various other patterns have been reported in literature as well [21, 78, 102, 106, 107, 149, 152, 159, 241]. The findings vary depending on the focus of the study as well as on the definition of the drainage pattern. Overall, common variants are a third middle right PV [241]

and a common trunk of the two left PVs [107, 159]. Kaseno et al. [106] observed a short common left trunk in more than half of 428 computed tomography (CT) scans of individual patients. In the detailed study of Marom et al. [152] four different patterns (1–2 ostia) on the left and ten different patterns (2–5 ostia) on the right side of the LA are distinguished.

The venous tissue of the PVs is covered by myocardial cells [85, 108]. These so-called sleeves have a variable length from the junction of the ostia and the left atrial body and are longer in the superior veins compared to the inferior veins [24, 88, 86, 202], which concurs with a higher rate of ectopic foci in the superior PVs [74]. The left superior PV (LSPV) was shown to have the longest sleeve, followed by the right superior PV (RSPV), left inferior PV (LIPV) and right inferior PV (RIPV) (41 vs. 30 vs. 21 vs. 13 mm) [24] and no significant difference between controls and AF patients was found. Measurements from Hassink et al. and Saito et al. confirmed the order of different length in PV sleeves, but experienced shorter extension of myocardium into the PVs (7.2-10.9 mm [81] and 6.0-14.8 mm [202]). Hassink et al. [81] also found the sleeves in the AF group to be longer than in controls (10.4 vs. 8.7 mm), whereas Saito et al. [202] did not find a significant difference.

2.1.3 *Atrial isthmuses and interatrial septum*

In the RA, the area between the IVC and the tricuspid valve forms an isthmus [19, 85]. This region is linked to macro-reentries in atrial flutter and is thus often target of ablation therapy [19], as it has a slower conduction velocity in these patients [55]. The LA hosts the mitral isthmus in the region between the mitral valve and the LIPV, which may also be target of ablation in AF patients [263].

The interatrial septum includes an electrically isolating layer [3, 84, 131]. Both sides of the septum are covered with conductive myocardium, except in the area of the fossa ovalis, where only the ring around the fossa ovalis is conductive.

2.2 Geometric models of the atria

Geometrical atrial models can be divided into different groups. One group consists of very detailed models of specific parts of mammal atria, most often of regions of the RAA, CT and PMs as well as the PV ostia (e.g. [22, 53, 271, 273]). Another group includes 3D models of human atria. This group can be subdivided into surface and volumetric models. Both model types represent a geometry in three dimensions, but surface models cannot reflect the finite wall thickness of the atria. The models represent either generalized atrial shapes (e.g. a two-sphere "peanut"), the anatomy of a single human derived from image data (magnetic resonance imaging (MRI) or CT) or very recently reflect patient-specific atrial anatomies. Table 1 provides an overview of published 3D models of the atria and their properties.

Besides atrial models created for electrophysiological simulations, further atrial models, partly comprising fast conducting myocardial structures, were published without performing electrophysiological simulation [43, 165, 173, 200, 232, 258].

Geometric atrial models usually reflect the normal atrial anatomy, with four PVs and an average literature-based wall thickness, if this information could not be derived from the image data. An inconsistency exists in the modeling of the atrial septum, which is modeled either as fully conductive, or including an isolating layer (see Table 1). On the other hand, modeling of interatrial bundles is more consistent, as models commonly at least include the connection via BB and the CS (Table 1).

2.2.1 *Emerging imaging and segmentation technology*

Recent advances in cardiac imaging allow the creation of patient-specific atrial models from various data entities, such as CT [49, 50, 94], 4D CT [156], cone-beam CT [150], MRI [258], and TEE [252]. These advances will enable the use of such models for electrophysiological simulations accompanying the clinical workflow [124, 48].

New image segmentation techniques also allow the patient individual determination of the PV variant [47, 78, 107], which will support the generation of detailed personalized geometrical atrial models. Advances in MRI enable in-vivo imaging of atrial wall thickness, which in future could augment personalized atrial models [165]. Imaging atrial fiber orientation in-vivo using diffusion tensor MRI, is not yet possible, although becoming feasible for the ventricles [238], because MRI resolution is in the range of atrial wall thickness and partial volume effects would therefore outweigh real data.

Another rising aspect is the generation and utilization of cardiac atlases and statistical models [264]. Atlases are generated from a multitude of image data and can be used to find a representation for the mean anatomy [173] and to show the variability of certain anatomical features [140]. Data for the generation of cardiac atlases as well as individual atrial models can be found in web-based databases (Cardiac Atlas Project (CAP) [7], Anatomical Model Database (AMDB) [65]). Statistical mean models are already used for cardiac image segmentation, but may in future also play a role in therapy planing and clinical training.

2.3 Fibers and bundles

Atrial fiber orientation with high anisotropy or other disturbances was shown to be linked to the onset and sustaining of AF [96, 177]. Preferred orientation of atrial

Table 1 3D geometrical atrial models

References	Basis	Species	Comp.	Geo.	Mesh	EPM	Prop.	Fibers	Sep.	Heterogeneities		Ext.
Lorange et al. [141]		Human (CT)	Four chamber	Surf-2D	Voxel	n/p	eikonal	–	c	–		ECG
Ellis et al. [54]		Generic	Biatrial	Surf-2D	Icosahedral	n/p	n/p	–	n/p	–		Abl
Gray et al. [70]		Generic	Two spheres	Surf-3D	Cubic	[61]	[70]	–	c	–		
Freudenberg et al. [62]		Visible female	Biatrial	Vol	Voxel	n/p	CA	–	c	CT	(G/-/-)	
Harrild et al. [80]		Human (MRI)	Biatrial	Vol	Hexahedral	Nyg	MD	B	i	BB, CT, PM, IS, FO	(G/CV/-)	
Werner et al. [259]		Visible man	Four chamber	Vol	Voxel	n/p	CA	V	c	–		ECG
Vigmond et al. [249]		Generic	Two spheres	Surf-3D	Cables	[186]	[249]	ML	i	BB, CT , PM, CS, FO	(G/-/-)	
Zemlin et al. [266]		Visible female	Biatrial	Surf-3D	Triangular	CRN	[266]	ML	c	CT, PM	(G/CV/-)	
Blanc et al. [14]		Generic	Two spheres	Surf	Voxel	[11, 143]	MD	–	c	–		
Virag et al. [251]		Human (1, MRI)	Biatrial	Surf-3D	Triangular	CRN	MD	–	i	BB, CT, FO	(G/CV/-)	
van Dam et al. [35]		Human (1, MRI)	Biatrial	Surf-3D	Triangular	n/a	FM	–	c	–		
Jacquemet et al. [37, 99, 100, 195–197, 243]	[251]	Human (1, MRI)	Biatrial	Surf-3D	Cubic	CRN	MD	ML	i	BB, CT, FO	(G/-/-)	Abl, ECG
Seemann et al. [219]		Visible female	Biatrial	Vol	Voxel	CRN	MD	B	c	BB, CT, PM, AVR, APG, SN	(G/CV/EP)	
Ridler et al. [190]		Human (1,CT)	Biatrial	3D	Cables	[186]	MD	Yes	i	CS, FO, CS	(G/-/-)	
Dokos et al. [46]		Generic	Two spheres	Surf-2D	Triangular	[193]	n/p	–	c	–		
Kuijpers et al. [128]	[35]	Human (1, MRI)	Biatrial	Surf-3D	Triangular	CRN	BD	–	c	–		
Gong et al. [66]	[80]	Human (averaged)	Biatrial	Vol	Hexahedral	CRN	n/p	B	i	BB, CT, PM, CS, FO, IS	(G/CV/-)	
Plank et al. [178]	[219]	Visible female	Left atrium	Vol	Voxel	CRN	MD	V	n/a	–		
Tobón et al. [233–236]	[80]	Human (1, MRI)	Biatrial	Surf-3D	Triangular	Nyg	MD	ML	i	BB, CT, PM, CS, IS, FO	(G/CV/-)	Abl
Wieser et al. [261, 262]	[232]	Human (1, MRI)	Biatrial	Surf-3D	Triangular	[186]	MD	–	i	BB, CT, CS, FO	(G/CV/-)	
Reumann et al. [188]	[219]	Visible female	Biatrial	Vol	Voxel	CRN	CA	B	c	BB, CT, PM	(G/-/-)	Abl
Kharche et al. [110]	[219]	Visible female	Biatrial	Vol	Voxel	CRN	CA	B	c	BB, CT, PM, AVR, APG, SNs	(G/CV/EP)	
Krueger et al. [126]	[259] [219]	Visible man Visible female	Biatrial	Vol	Voxel	CRN	MD	B	c	BB, CT, PM	(G/CV/EP)	
Krueger et al. [123, 226]		Human (2, MRI)	Biatrial	Vol	Voxel	CRN	MD	B	c	BB, CT, PM, AVR, APG	(G/CV/EP)	Abl, ECG

Table 1 continued

References	Basis	Species	Comp.	Geo.	Mesh	EPM	Prop.	Fibers	Sep.	Heterogeneities	Ext.
Abed et al. [1]		Visible man	Biatrial	Vol	Voxel	[1]	MD	–	n/p	BB, CT, CS, APG	(G/-/-)
Krueger et al. [124]		Human (15, CT, MRI)	Biatrial	Vol	Voxel	CRN	MD	VL	c	BB, CT, PM, IS, AVR, APG	(G/CV/EP)
Lu et al. [142]		Human (1, MRI)	Four chambers	Vol	Spheroidal	Nyg	CA	–	n/p	BB, CT, PM, IS, FO	(G/-/-) ECG
Aslanidi et al. [6]	[219]	Visible female	Biatrial	Vol	Voxel	CRN	[6]	BS	c	BB, CT, PM, SN	(G/CV/EP) ECG
Cristoforetti et al. [33]		Human (1, CT)	Left atrium	Surf	Triangular	CRN	n/p	–	n/a	–	
Ridler et al. [191]	[190]	Human (1, CT) (dog size)	Biatrial	3D	Cables	[114]	MD	–	i	CT, CS, FO	(G/-/-)
Burdumy et al. [16]		Human (4, CT)	Biatrial	Vol	Voxel	CRN	CA	–	c	–	
Zhao et al. [272]		Sheep (1, microscopy)	Biatrial	Vol	Voxel	[57]	MD	V	c	BB, CT, PM, PV	(G/-/-)

EPM electrophysiological model, *CRN* model of Courtemanche et al. [31], *Nyg* model of Nygren et al. [168], *Comp.* compartments, *Prop.* propagation model, *Sep.* septum, *B* bundles, *V* volumetric, *ML* mono-layer, *VL* various layers, *BS* bundles and SN, *Ext.* model extension, *Abl* ablation lesion model, *ECG* ECG is computed, *Surf* surface model, *Surf-3D* 3D surface model, *vol* 3D volumetric model *CA* cellular automaton, *MD* monodomain, *BD* bidomain, *i* isolating, *c* connective, *n/a* not applicable, *n/p* not specified, *IS* right atrial isthmus, *AVR* atrio-ventricular ring, *APG* appendages, *G* structures in geometry, *CV* structures have different conductivity, *EP* structures have different electrophysiology

myocytes (myocardial fiber orientation) in the human atria is characterized by multiple overlapping, joining and separating fiber sheets and bundles. Some of the bundles have strong anisotropy and significantly influence the atrial depolarization sequence [13, 38, 151]. In the RA, the CT is the most prominent bundle and runs from the inferior vena cava (IVC) to the SVC while diminishing in width (9.1 vs. 6.1 mm) [205]. 15–20 PMs arise perpendicularly from the CT towards the muscular ring of the tricuspid valve [253]. The superior PM, so-called septum spurium, marks the beginning of the circular oriented myocardial fibers of the tip of the RAA and is thicker compared to the other PMs (4.2 mm vs. 1–3 mm) and shorter [205]. The inferior PMs encircle the orifice of the CS. From the circular fibers surrounding the SVC an epicardial fiber layer is extending over the smooth portion of the RA between the caval veins, crosses the CT epicardially and joins the fibers of the PMs [175].

Fiber orientation in the LA is made up of two myocardial layers overlapping each other transmurally. The septo-atrial bundle lies in the subendocardium and the septo-pulmonary bundle runs subepicardially [87]. The PV ostia and the atrio-ventricular valves are encircled by myocardial fibers [161]. An abrupt change of fiber direction can be present at the PV ostia [89]. The most comprehensive reviews of atrial fiber orientation can be found in Refs. [84] and [87].

2.3.1 Modeling atrial fibers

Fiber orientation can be included based on published anatomical observations (described above) into atrial models manually [80, 100, 219, 235, 249] or semi-automatically/rule-based [83, 123, 124, 126, 177, 200, 259, 266]. All models have in common, that surface-3D models cannot fully reproduce the complex multi-layer fiber arrangement described above. An example for rule-based, volumetric atrial fiber orientation is pictured in Fig. 1. In addition, more detailed animal models of specific atrial regions include fiber orientation derived from high-resolution imaging [22, 272, 273]. It has been shown, that some of the prominent bundles may be visible in high-resolution CT scans [208, 209]. This yields the possibility to include patient individual sizes of these structures in atrial models in the future. Recently, semi-automatic methods were presented to incorporate fiber orientation in patient-specific atrial models [83, 123, 124, 126].

3 Electrophysiology

3.1 General atrial electrophysiology

The resting membrane voltage of a human atrial myocyte is about −80 to −90 mV. An external stimulus leads to the

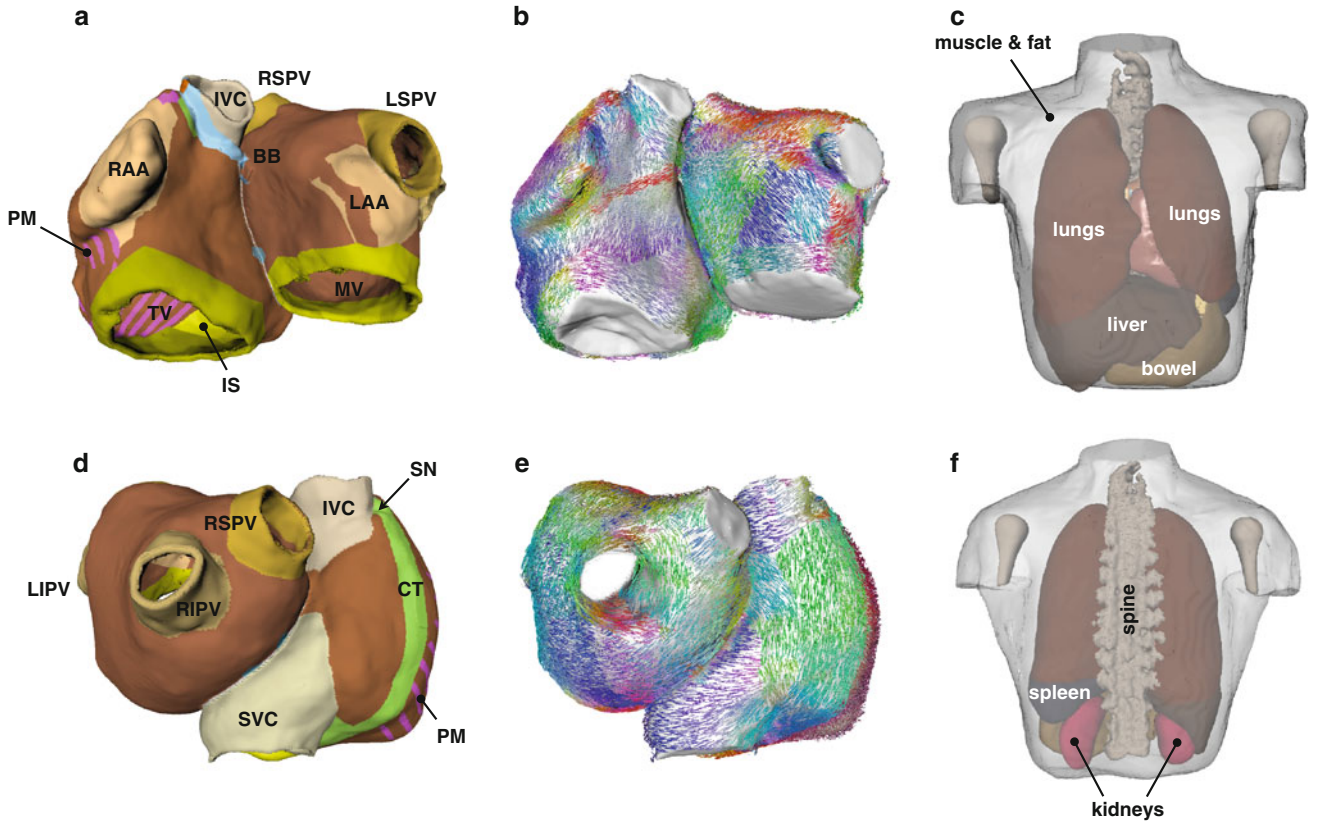

Fig. 1 **a**, **d** Anatomical model of an AF patient with structures relevant for EP simulations (*colored*). **b**, **e** Rule-based volumentric fiber orientation in the atrial model [124]. Orientation of fibers is color-coded. **c**, **f** Anterior and posterior view of a thorax model of a volunteer with segmented organs [123]

initiation of a characteristic action potential (AP). The AP starts with the opening of fast Na^+ channels, which are rapidly inactivated causing the refractory period. After the overshoot, fast repolarizing K^+ outward currents lead to a decrease of the transmembrane voltage. This process is prolonged by a slow Ca^{2+} inward current. Afterwards, repolarizing delayed rectifier K^+ channels restore the resting membrane voltage. The duration of an atrial AP ranges between 200 and 300 ms. The differences in ion concentrations of Na^+ and K^+ between intra- and extracellular space are maintained by energy-consuming ion pumps and exchangers.

The pacemaker of the whole heart is the SN, where specialized cells spontaneously activate the surrounding tissue. There, a hyperpolarization-activated funny current I_f in combination with other currents as e.g. the sodium calcium exchanger slowly depolarize the membrane, which results in the initiation of an AP [129]. In the different regions of the right and left atrium, AP shape and duration (APD) are heterogeneously distributed. Differences between the APs of the RAA, CT, PM and atrio-ventricular ring as well as between RA and LA were investigated in canine atria [56, 134]. Furthermore, AP parameters of human atrial myocytes such as, e.g., APD_{90} or effective refractory period (ERP) decrease with shorter diastolic intervals [111, 265].

3.2 Electrophysiological models

On the cellular level, the mathematical description of cardiac electrophysiology is mostly based on the work of Hodgkin and Huxley [91], who introduced a mathematical model of neural cells in 1952. Depending on the model's level of detail, several non-linearly coupled ODEs describe the cell membrane and the different ion concentrations. The change of transmembrane voltage V_m is calculated as follows:

$$dV_m/dt = -(I_{ion} + I_{stim})/C_m, \quad (1)$$

where I_{ion} is the sum of ion currents flowing through channels, pumps and exchangers across the membrane, I_{stim} an externally applied stimulus current and C_m the membrane capacity. The different ion currents I_x are computed using conductivities g_x scaling the amplitude and the product of gating variables γ_i describing the open probability of the channels depending on V_m:

$$I_x = g_x \prod_i \gamma_i (V_m - E_{\text{Nernst,x}}), \quad (2)$$

$$\frac{d\gamma_i}{d_t} = \alpha_{\gamma_i}(1-\gamma_i) - \beta_{\gamma_i}\gamma_i, \quad (3)$$

where $E_{\text{Nernst},x}$ is the reversal potential of the ion type x and α_{γ_i} and β_{γ_i} are rate constants describing the transition from closed to open state and vice versa. Furthermore, intracellular calcium handling including formulations for the Ca^{2+} uptake and release of the sarcoplasmic reticulum are considered in current models. The setup and solution of the equations used in the models is shown more detailed in Ref. [59].

3.2.1 Modeling human atrial electrophysiology

The first models of human atrial electrophysiology are the ones published by Courtemanche et al. [31] and Nygren et al. [168] in 1998. Both models are mostly based on the same human experimental data. However, some of the formulations depend on experimental data of other mammals, where human data are missing. Although they have a similar base, the APs of the models have a different morphology (compare Fig. 2a). The Courtemanche model shows a spike-and-dome morphology, whereas that of Nygren et al. presents a more triangular shape. Furthermore, the APD_{90} restitution curves of both models differ (see Fig. 2b). At high basic cycle lengths (BCLs), the APD of the Courtemanche model is almost 70 ms longer and it decreases towards shorter BCLs, whereas that of the Nygren model decreases towards a BCL of 470 ms and then increases again. The differences and similarities of both models were compared in detail in e.g. Ref. [27, 169]. The Nygren model was refined by Maleckar et al. [148] in 2008, with a focus on improving the rate dependence of the AP and the formulations of repolarizing currents. The AP of the Maleckar model is similar in shape and duration to that of Nygren. The APD_{90} restitution curve is also similar to that of the previous model, although the APD is shorter and stagnates towards shorter BCLs. Also based on the Nygren model, Koivumäki et al. [119] added a more detailed atria-specific description of the sarcoplasmic reticulum considering spatial effects of Ca^{2+} uptake and release in 2011. As a consequence, the AP mainly differs from the Nygren model in the first half of the plateau phase. The APD restitution curve has a similar shape as the Courtemanche model although the APD is shorter in the Koivumäki model. Also in 2011, Grandi et al. [68] published a human atrial model that also focuses on intracellular Ca^{2+} dynamics. This model furthermore considers the impact of β-adrenergic and cholinergic stimulation on human atrial APs. Since it is based on a ventricular model of the same group [69], also the ionic bases for the differences between atrial and ventricular APs were investigated. The AP shows a similar shape as the Nygren-based models, but has an APD comparable to that of the Courtemanche model. The APD_{90} increases towards a BCL of 450 ms and then decreases again. The shape of the APs of the models and also the restitution properties can also be adapted to other models or experimental data, as e.g. shown in Ref. [230]. An overview of the model properties is given in Table 2.

3.2.2 Restitution properties

The models of human atrial electrophysiology show different restitution properties (see Fig. 3) of the conduction velocity (CV), ERP and WL ($WL = CV \cdot ERP$) when analyzed in a 1D tissue patch. These restitution curves are good indicators of the stability of reentrant circuits [112]. The intracellular conductivity is adjusted so that a CV of approximately 75 cm/s is obtained at a BCL of 1 s. In general, the CV decreases towards shorter BCLs. The Grandi model presents a rapid decline of the CV down to a BCL of 550 ms. Only the Courtemanche model presents an increase towards 500 ms and then decreases again. In contrast to the other models, the ERP of this model decreases towards short BCLs. The ERPs of the Nygren,

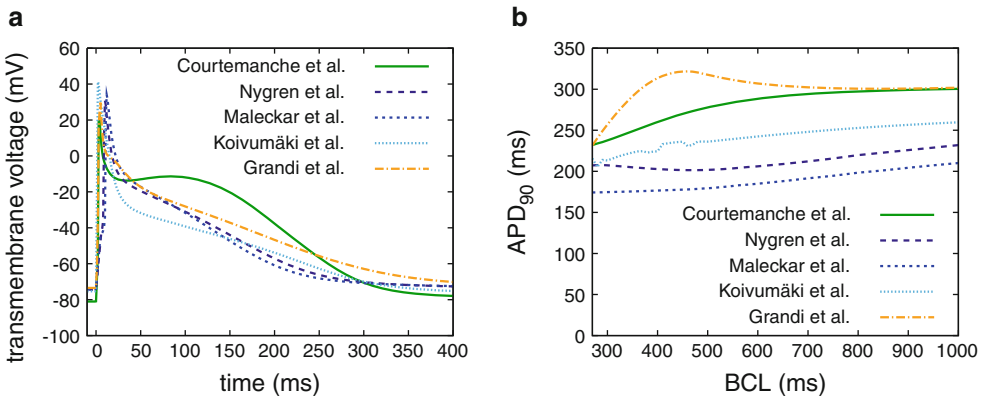

Fig. 2 **a** Action potentials and **b** APD_{90} restitution of the different models of human atrial electrophysiology

Table 2 Properties of models of atrial electrophysiology

Author	Reference	Transmembrane currents	Ca^{2+} Compartments	Intended investigations	Extensions	Parent model
Courtemanche et al.	[31]	Common[a]	Intracellular, extracellular	Rate-dependent adaptation of human atrial AP, block of I_{CaL} and I_{NaCa}	AF: [27, 32, 242, 268], long-term stability: [172]	[144]
Nygren et al.	[168]	Common[a]	Intracellular, dyadic cleft, cleft space[b], extracellular	Differences between rabbit and human atrial electrophysiology, especially repolarizing currents	AF: [27, 268]	[138]
Maleckar et al.	[148]	Common[a] + acetylcholine-activated K^+ current I_{KACh}	Intracellular, dyadic cleft, cleft space[b], extracellular	Rate-dependent repolarization of human atrial AP, coupling between myocytes and fibroblasts	acetylcholine: [148]	[168]
Koivumäki et al.	[119]	Common[a] + hyperpolarization-activated inward K^+ current I_f	Four spatially varying intracellular spaces, subsarcolemmal, extracellular	Detailed description of calcium dynamics and impact on AP morphology		[168]
Grandi et al.	[68]	Common[a] + I_{KACh} + Cl^- currents (background I_{bCl}, Ca^{2+}-activated $I_{Cl(Ca)}$)	Intracellular, dyadic cleft, subsarcolemmal, extracellular	Differences between human atrial and ventricular electrophysiology with focus on calcium handling	AF: [68], β-adrenergic: [68], acetylcholine: [68]	[69]

[a] Common to all models: fast Na^+ current I_{Na}, L-type Ca^{2+} channel I_{CaL}, transient outward current I_{to}, ultrarapid delayed rectifier K^+ current I_{Kur}, slow and rapid delayed rectifier K^+ current I_{Ks} and I_{Kr}, inward rectifier K^+ current I_{K1},Na^+ and Ca^{2+} background currents I_{bNa} and I_{bCa},Na^+/Ca^{2+} exchanger I_{NaCa}, $Na^+ - K^+$ pump current I_{NaK}, sarcolemmal Ca^{2+} pump current I_{pCa}

[b] Cleft space: cell surrounded by restricted space, where ions accumulate or deplete

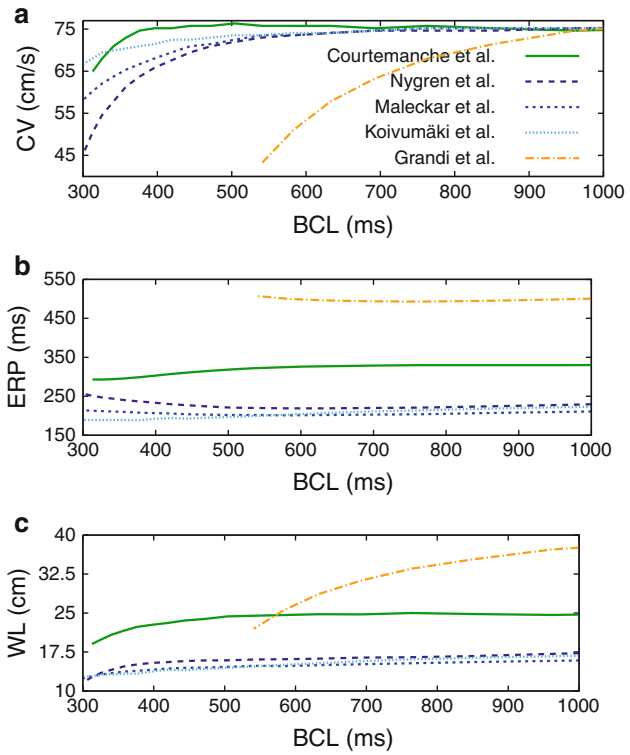

Fig. 3 **a** CV, **b** ERP and **c** WL restitution of the different models of human atrial electrophysiology

Maleckar and Koivumäki models are much shorter. The ERP of the Nygren and Maleckar model even increases towards short BCLs. The highest ERP is obtained by the Grandi model, which therefore can only be computed to BCLs down to 550 ms. The resulting WL decreases in all models towards shorter BCLs. The WL of the Grandi model is longer than that of the Courtemanche model. The Nygren-based models have the shortest WL indicating a more probable initiation and persistence of arrhythmias.

3.2.3 *Atrial heterogeneity*

In several computational studies, heterogeneities of atrial electrophysiology were investigated. However, all of these studies were based on animal experimental data, e.g. [56, 134]. In Ref. [186], a canine atrial model considering heterogeneous APs of the RAA, CT, PM and atrio-ventricular ring was developed. The same experimental data were used for the integration of these heterogeneities into the human atrial model of Courtemanche et al. in Ref. [219] and into the model of Nygren et al. in Ref. [235]. In Ref. [273], the human Courtemanche model was adapted to APs of the canine CT and a modified version of the Luo-Rudy model [185] was adapted to APs of the canine PM. Zhao et al. altered the model of Courtemanche et al. to reproduce APs from the CT [273]. In a recent computational study [6], the Courtemanche model was

modified to simulate different APs in the RAA, CT, PM and atrio-ventricular ring, as well as in the LA.

3.2.4 Sinus node

Although very detailed models of the SN of rabbits are reported [269], only few models of human SN exist. In Ref. [219], the Courtemanche model was modified based on a heterogeneous model of the rabbit SN [269]. Furthermore, Aslanidi et al. [6] used modifications of the Courtemanche model published by Chandler et al. [23] to simulate human SN APs.

4 Excitation propagation

4.1 Propagation properties

The myocardium is built mainly of discrete cardiomyocytes. These myocytes are surrounded by the extracellular space and are coupled electrically by gap junctions. A transmembrane voltage difference in adjacent cells generates a current through gap junctions and through the extracellular space in such a way that the activation can spread. Both the intracellular and extracellular conductivities show anisotropic behavior allowing a faster excitation propagation along the main axis of the cell than across.

4.1.1 Activation pattern during sinus rhythm

The physiological excitation of the heart driven by the SN is called sinus rhythm. The frequency adaptation of the SN is controlled by the autonomous nerve system and by hormones [15]. After activation of the SN, the fast right atrial pathways, i.e. CT and PM, conduct excitation preferentially towards the atrioventricular region. During that phase the RA becomes depolarized [13]. At the same time, BB conducts the excitation towards the LA. Finally, the whole atrium gets depolarized after approximately 100 ms. All conduction pathways are characterized by a large conductivity along the fiber direction leading to a fast conduction velocity along their main axis.

4.1.2 Conduction velocity and anisotropy

The measured longitudinal conduction velocity (CV) in the atrium lies between 51 and 120 cm/s for non-AF patients (see Table 3). Under pathological conditions the variance increases to values between 37 and 133 cm/s. With age, the CV decreases [120]. In general, the CV along the conduction bundles is faster than in the working myocardium. Only little is known about anisotropic features of the CV. Spach et al. [227] measured an averaged ratio of 4.76:1 in the human atrium, but it is probably less pronounced since this measurement included conduction pathways. In CT, an anisotropy ratio of around 8:1 was described [201].

4.2 Modeling excitation propagation

Commonly, excitation conduction is calculated with macroscopic approaches describing the atrial tissue as a continuum [6, 35, 80, 95, 113, 160, 188, 199, 219, 233, 249, 251]. One computational node is reproducing the properties of several real myocytes. The used models can be divided into three degrees of complexity: rule-based methods (i.e. cellular automaton), simplified propagation models (e.g. the shortest path algorithm and eikonal models) and models of the electrical current combined with detailed electrophysiological descriptions (e.g. mono- and bidomain models).

4.2.1 Rule-based method

Cellular automata (CA) have a finite number of states to describe electrophysiological properties. Very early studies used this approach [160] as the computational cost is very low. Newer CA can consider tissue anisotropy and appropriate wavefront curvature [199] as well as rate-dependent APD adaptations [188]. The disadvantage of the CA is the limited possibility to adjust electrophysiologically relevant parameters and the lack of electrotonic interactions.

4.2.2 Simplified conduction methods

The shortest path algorithm is the most simple propagation model as it does not include any electrophysiological state. In combination with a precise geometrical model, it can be used to illustrate routes of excitation [35]. Eikonal models are still simplified approaches but consider anisotropy and electrophysiological states [42, 122]. These models can be implemented efficiently using e.g. a multi-front fast-marching algorithm. Eikonal models have been used recently to investigate reentrant behavior of atrial tissue [95]. Also here the disadvantage is that cellular measurement data can poorly be integrated into the model.

4.2.3 Detailed reaction-diffusion models

Mono- and bidomain models consider the electrical current of ions between adjacent cells [29, 82]. The bidomain model is taking into account the current in intra- and extracellular space as well as through gap junctions and the cell membrane. It is based on the two Poisson equations:

$$\nabla \cdot (\sigma_e \nabla \Phi_e) = -\beta I_m - I_{se} \quad (4)$$

$$\nabla \cdot (\sigma_i \nabla \Phi_i) = \beta I_m - I_{si} \quad (5)$$

Table 3 Conduction velocities reported in the literature from measurements in human tissue

Study	Subjects	Region	Longitudinal (cm/s)	Transversal (cm/s)	BCL (ms)	Condition
[55]	9	septum	58–61		300–600	H
		RA FW	58–64			
		isthmus	51–55			
[79]	12	RA FW	88		SR	H
[136]	21	RA septum	96–98		200–500	H
		RA FW	94–100			
[227]	49	PM	70	8.2	800	H
[45]	20	RA	120		SR	H
	20	LA	120		SR	H
[105]	16	RA FW	83		1006	CAB
			77		500	
[55]	9	septum	50–54		300–600	Aflut
		RA FW	53–57			
		isthmus	37–42			
[136]	25	RA septum	86–91		200–500	Aflut
		RA FW	91–98			
[212]	8	isthmus	77		240	Aflut
		RA smooth	108			
		PM	133			
[222]	9	isthmus	70		243	Aflut
		RA sup	120			Aflut
		RA lat	110			Aflut
		RA septum	110			
[45]	20	RA	80		SR	OSA
		LA	90			
[255]	5	RA, LA post & roof	108		SR	AF/FAT
		RA, LA post & roof	86		500	
		RA, LA post & roof	77		300	

FW free wall, *Aflut* atrial flutter, *FAT* focal atrial tachycardia, *OSA* obstructive sleep apnea, *H* no arrhythmia, *CAB* coronary artery bypass.

with the intra- and extracellular potentials Φ_i and Φ_e, respectively, the corresponding conductivity tensors σ_i and σ_e, the transmembrane current density I_m, the membrane surface to cell volume ratio β, and externally applied current sources I_{si} and I_{se} in the intra- and extracellular domain, respectively. I_m is the sum of capacitive and ionic membrane currents:

$$I_m = C_m \frac{dV_m}{dt} + I_{ion} \quad (6)$$

with I_{ion} being the sum of all transmembrane currents I_x from Eq. 2.

Under the assumption of equal anisotropy ratios, this model can be reduced to the monodomain model calculating the current through the intracellular space and through gap junctions:

$$\nabla \cdot (\sigma \nabla V_m) = \beta \left(C_m \frac{dV_m}{dt} + I_{ion} \right) \quad (7)$$

In both the cases, the model of current is connected in each computational node to detailed electrophysiological models of e.g. Courtemanche or Nygren. Most of the atrial modeling studies have used the monodomain model [6, 80, 113, 219, 233, 249, 251]. Figure 4 illustrates the propagation simulation on a schematic 2D patch and on a realistic 3D geometrical model using the monodomain method. The disadvantage of mono- and bidomain modeling is the large computational cost and the large number of parameters in the model that cannot be determined with sparse measurement data.

4.2.4 *Conduction velocity and anisotropy*

Many modeling studies lie within the range of measured conduction velocities (36 to 130 cm/s) and also consider the velocity differences in different tissue types (e.g. isthmus 36 cm/s, atrial myocardium 65 cm/s, bundles 210 cm/s in [66]). In addition, anisotropy ratios of the CV have been

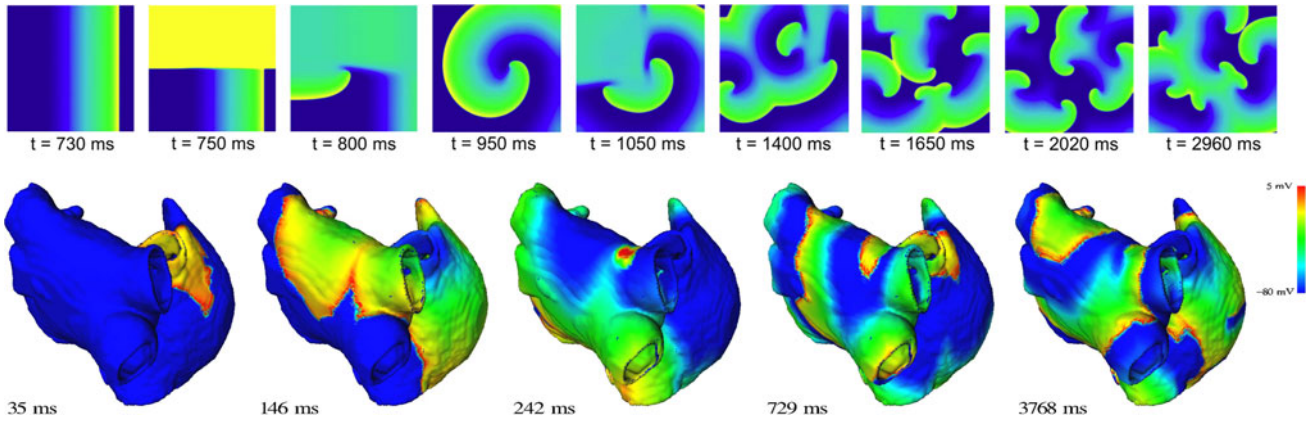

Fig. 4 *Top row* simulation of AF rotors in a 2D patch of atrial tissue [218]. Rotors are generated using a cross-field stimulus protocol. *Bottom row* example of simulation of AF in a 3D model. AF is triggered by ectopic activity in the RSPV (241 ms) after initial sinus rhythm (35 ms)

set e.g. to 1.9:1 [6], 2.4:1 [113, 133] or 3:1 [266] in the working myocardium and to e.g 6:1 [262] or 9:1 [100, 219] for the conductivity in the conducting pathways. The working myocardium is often treated isotropically since fiber orientation information in the human atrium is rarely included in the models (Table 3).

4.2.5 Stimulation of tissue

In order to simulate sinus rhythm, the reported approaches are either to apply an intracellular stimulus current in the region where the SN is located [80, 251] or to set nodes close to the SN to be self-excitatory cells [6, 219]. A crossfield stimulation can be used to generate a single rotor in the tissue (see Fig. 4 upper row, left). Here, a first planar excitation is initiated and then in the half refractory/half excitable period a perpendicular second current is applied [218]. In order to generate multiple reentrant waves, pulse trains can be used reproducing ectopic focal activity. These pulse trains can be with constant position and rate e.g. in the pulmonary vein [188] or vary in position and rate to more easily produce multiple reentries (see Fig. 4 upper row, right).

5 ECG

5.1 Computation of ECG and electrograms

Body surface potentials are commonly computed in a two-step approach. In a first step, transmembrane voltages are simulated in the atrial models using an arbitrary excitation propagation model (see Sect. 4 excitation propagation). From the transmembrane voltages V_m the impressed current sources I_{imp} can be calculated

$$I_{imp} = -\nabla \cdot (\sigma_i \nabla V_m). \tag{8}$$

In a second step, Poisson's equation as the parabolic part of the bidomain formulation [82, 184] is solved

$$\nabla \cdot [(\sigma_i + \sigma_e)\nabla \Phi_e] = I_{imp}. \tag{9}$$

Thereby Dirichlet and Neumann boundary conditions are set for the reference potential and the thorax-air boundary. Considering these conditions, the bidomain formulation is transformed into a linear set of equations using either the finite element method (FEM) (e.g. [109, 125, 259]) or the boundary element method (BEM) (e.g. [142, 171]). The FEM has the advantage that it can consider anisotropy within the organs (e.g. skeletal muscle fiber orientation), whereas the BEM is computationally more efficient. Measurements of the organ conductivities show a large variability leading to some uncertainties in solving the forward problem [109]. ECG signals can then be extracted at surface nodes of the thorax model. In order to compare simulated and measured signals, the measurement electrodes need to be tracked with respect to the torso model during ECG recording [123].

Intracardiac electrograms can be simulated using the methods described above [256] or by computing pseudo-electrograms

$$\Phi_e(r,t) = \frac{1}{4\pi\sigma_e} \int \left(dr' \frac{I_m(r',t)}{|r-r'|} \right), \tag{10}$$

where r is the electrode location vector, r' the current source location vector and I_m the transmembrane current per unit area of tissue surface [236, 251].

5.2 Characteristics of the P- and Ta-wave

The atrial depolarization sequence can be seen in the body surface ECG as the P-wave. The signal of the P-wave is strongest in the Einthoven II lead and shows a Gaussian-like shape with a maximum amplitude of 0.25 mV. The P-wave has a smooth contour and is monophasic positive in

lead II, inverted in aVR and often biphasic in V1 [216]. Left atrial enlargement may cause a bifid P-wave (P mitrale) and right atrial enlargement may cause a peaked P-wave (P pulmonale) [216]. Inversion of the P-wave is caused by ectopic triggers and a variable morphology is caused by multifocal arrhythmias [216].

The duration of the P-wave (PWd) reflects the time of complete atrial depolarization. AF patients often have a longer P-wave duration (120 ms) compared to controls (100 ms) [44, 71], which can be used to detect AF based on the P-wave duration [39]. Nevertheless, automatic detection based on P-wave analysis shows only moderate specificity and sensitivity [28, 63]. The integrated body surface potential maps (BSPMs) of the P-wave show a dipole on the front chest from the right shoulder to the left hip with the zero potential line crossing from the left upper chest to the lower right chest [135, 158, 224]. The body surface potential distribution can vary depending on the site of the origin of atrial activity [224].

Atrial repolarization is usually not visible in the body surface ECG, as the repolarization signal is occluded by the much larger QRS complex due to the ventricular depolarization. In patients with third degree AV block, the repolarization signal can be measured. The polarity of the so-called Ta-wave is inverted compared to the P-wave and has a smaller amplitude [92].

Right-to-left atrial conduction varies between individuals [13, 90, 93, 132, 151, 179]. The most common sites of septal breakthrough are over Bachmann's bundle at the anterior side of the LA, the musculature of the CS and the region near the fossa ovalis [13, 38, 93, 131]. The individual interatrial conduction can be deduced from the polarity of the vectorcardiogram (VCG) [93].

5.3 Simulation of atrial ECG

Only few groups have simulated body surface ECG from bi-atrial electrophysiological simulations. The first efforts go back to the early 1990s, when Kafer examined interatrial conduction in the VCG with a computer model [103]. Later on, the first four chamber simulations with ECG computation became computationally feasible [141, 259].

Van Dam, van Oosterom, and Jacquemet computed the P-wave and concentrated on volume conductor effects [36] and showed that an equivalent double layer source model was sufficient to reproduce a measured P-wave [171]. Later on, Jacquemet et al. examined the potential of the VCG to characterize AF using the methods introduced earlier [98].

Recently, more groups started to simulate the P-wave and body surface potentials from atrial depolarization. In two patient models the atrial ECG was computed. The generated P-waves were compared to measured P-wave signals from the same patients [123]. Figure 5 provides an example of the comparison between simulated and measured atrial electrical signals, which correspond on multiple scales. The torso and atria were segmented from MRI data of the patients and a number of organs in the torso were distinguished. Lu et al. [142] were able to compute a reasonable P-wave using a generic homogeneous thorax model. Similar work was done by Aslanidi et al. [6], although they incorporated the lungs into their model and utilized a different mathematical approach.

Furthermore, the computation of the P-wave was recently used to test influences of clinical therapies. Thereby the influence of hemodialysis therapy on atrial electrophysiology in a heterogeneous atria and thorax model was evaluated and a P-wave prolongation due to the therapy was revealed [125] (see also Sect. 8.2). In this study, also the atrial repolarization was less uniform during hypokalemia resulting in a larger Ta-wave amplitude.

The influence of the conductivity of different organs on the computed P-wave was evaluated, showing that muscle, blood, lungs and fat were the organs with the greatest sensitivity for the P-wave morphology [109]. Uncertainties in the organ conductivities can be predicted using a fast principal component analysis (PCA) based method [254].

6 Patient measurements for model validation

As described above, electrophysiological models are typically built on the ion channel level, based on voltage clamp or patch clamp techniques. Wherever available, human data are used, but the remaining channels are modeled from animal data. Although in many cases animal data may give a good approximation for humans, several uncertainties remain. Apart from that, a good parametrization on the single-cell level does not guarantee that the model resembles macroscopic excitation patterns in the atria, because coupling between the cells may influence excitation propagation. Therefore, it is of interest to obtain macroscopic measurements from patients or healthy subjects, and if possible also to compare them to properties of atrial models.

Patient data of interest are frequently acquired during EP studies, especially electrograms measured with multi-electrode catheters. The first step is to quantitatively analyze such data. In a second step, such measurements can be compared to model simulations. Furthermore, optical measurements allow for visualizing excitation in tissue patches, but are restricted to animal experiments so far.

6.1 Substrate characterization from electrophysiological studies

Electrophysiological studies are performed by inserting one or several catheters into the atria, most of which have

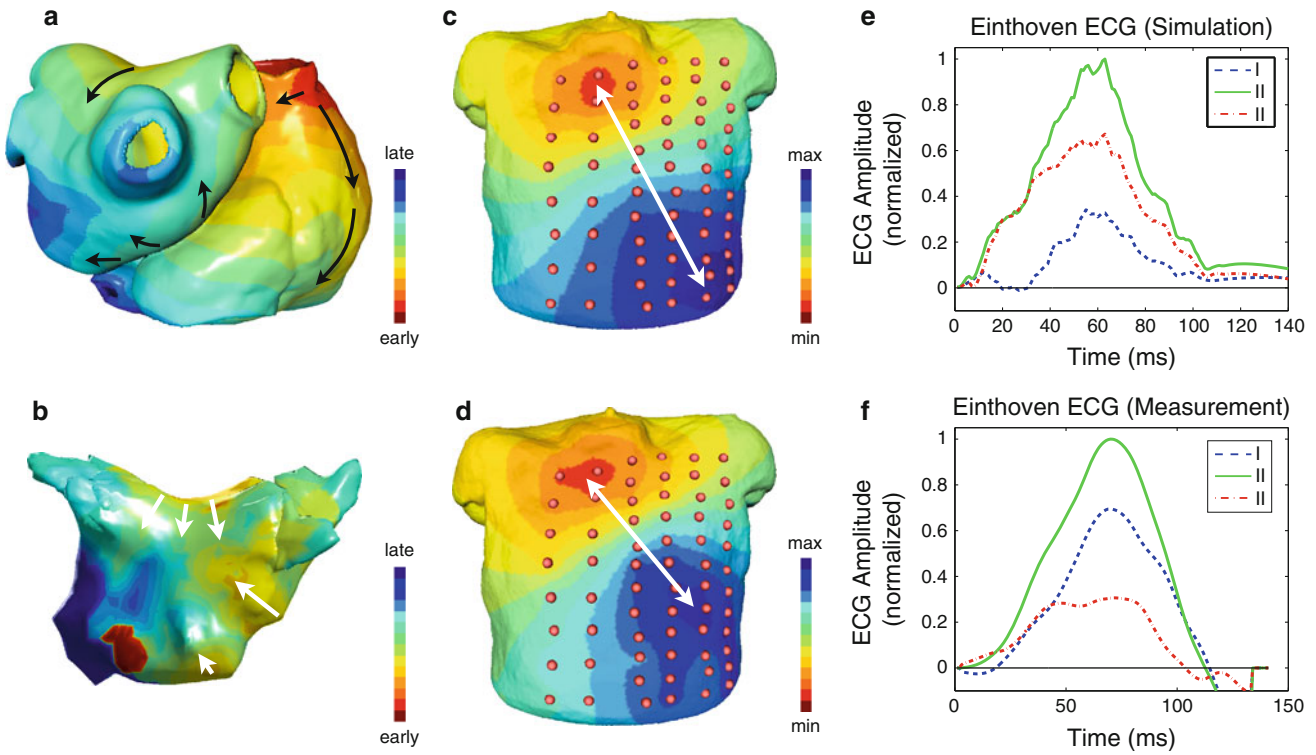

Fig. 5 **a** Simulated activation times in an atrial model. *Black arrows* indicate preferred conduction routes. **b** Measured local activation times in a left atrium. *White arrows* indicate preferred conduction routes. **c** Body surface potentials integrated over a simulated P-wave. *White arrow* marks the dipole from atrial excitation. **d** Body surface potentials integrated over a measured P-wave (same subject as in (**c**)). *White arrow* marks the dipole from atrial excitation. **e** Simulated Einthoven ECG (*dotted blue* lead I, *solid green* lead II, *dashed red* lead III). **f** Measured Einthoven ECG (same subject as in (**e**)). The simulation approach is similar to the one used in Refs. [123, 125], but data were acquired from different individuals here

multiple electrodes for recording electrical activation of the surrounding tissue [2, 213, 223]. It is further possible to apply a stimulation current via certain electrodes to induce an excitation wave, if the underlying tissue is not refractory. From such measurements, relevant data for atrial modeling can be obtained.

Catheters do not measure transmembrane voltages, but the extracellular potential difference between two electrodes that shows up during depolarization at the wave front. There are techniques to estimate APD from such intracardiac electrograms using the activation recovery interval [157]. However, because repolarization in the atria is slower than in the ventricles, repolarization currents are weaker, which makes the method more challenging in the atria. Vigmond et al. demonstrated an accuracy of around 40 ms for atrial APDs [250].

For simulating arrhythmias, it is even more important to determine the ERP. This is done during electrophysiological studies by programmed S1–S2 stimulation. An initial train of driving stimuli at cycle length S1 is followed by a shorter coupling interval S2. At a distant location, it is determined if the S2 pulse generated an excitation wave. In this case, the stimulation protocol is repeated with a shortened S2 until the S2 pulse falls into the refractory period. This way, atrial ERPs of 233 ms for the LA and 226 ms for the RA were measured at an S1 cycle length of 440 ms [194]. Such measurements can be combined with measurements of other excitation properties, such as electrogram voltage, degree of fractionation, conduction time, or CV [45].

CV measurements during EP studies are normally approximated from interpolated local activation maps. From the time delay and spatial distance between two or more points along the steepest gradient, the CV is estimated [45, 120, 121, 211]. More advanced techniques are based on vector field analysis of activation maps or data from epicardial electrode arrays [9, 10, 60]. Interpolation of atrial activation time fields based on sparse data was performed using radial basis functions [154]. Neither beat-to-beat variations in CV nor changes in the excitation pattern during map acquisition are considered because the activation map is recorded over many cardiac cycles. CV measurements on single wavefronts in the human RA were performed using epicardial electrode arrays during open-heart surgery [79]. A single-shot measurement of CV during EP studies was demonstrated for plane wavefronts using a circular mapping catheter [256]. With the same

technique, CV restitution was determined from pacing at different cycle lengths [255].

6.2 Comparison of models and clinical measurement

With patient data available, the outcome of atrial simulations can be compared to the measured data. Total activation times of the atria were simulated in a monolayer model generated from an MRI scan of a single patient. Simulated activation times for stimulation at different locations were comparable to mean P-wave durations from nine subjects [67, 262]. The average deviation over all stimulus sites was 8 ms. Stimulation protocols from electrophysiological studies were reproduced in silico on isotropic anatomical geometries derived from CT scans [16]. The propagation direction at catheter measurement sites in the LA deviated by 15° on average.

6.3 Optical mapping

Excitation in cardiac tissue can be visualized using voltage-sensitive fluorescent dyes [51, 52]. The fluorescence signal depends on the local transmembrane voltages and thus allows to image relative changes in tissue excitation. The dye is typically excited by a laser in the 532 nm range, and the resulting fluorescence signal is recorded by a CCD camera. With such data available, simulated excitation propagation can be compared to measurements.

Cherry et al. [26] demonstrated optical mapping of AF in tissue preparations from isolated perfused canine atria. Under the influence of acetylcholine, a sustained mother rotor was observed and compared to simulated data. Arora et al. [4] visualized arrythmogenic substrate in pulmonary vein preparations with conduction slowing in the proximal part and reentrant loops. Umapathy et al. [247] mapped stable rotors in monolayers of murine atrial tissue. Such studies are helpful to validate the dynamic evolution of 2D and 3D atrial simulations.

Kalifa et al. [104] presented a steerable cardio-endoscope for fluorescence mapping in the intact LA. Different propagation patterns were recorded in sheep hearts that had undergone a stretch-induced AF model. Although such measurements in the intact atrium are a step towards clinical patient measurements with optical mapping, a critical limitation is the phototoxicity of currently available fluorescence dyes [104].

7 Modeling atrial pathologies

The major application of human atrial models is to investigate atrial flutter and fibrillation. In 2008, Jacquemet et al. have published a comprehensive review article about the numerical modeling of atrial arrhythmias [97]. Since then, further atrial arrhythmia modeling work considering realistic atrial geometry was published [6, 33, 142, 178, 188, 191, 233–236]. In this review article, we want to focus on modeling the changes in electrophysiology and structure favoring the initiation and continuation of atrial arrhythmias. Therefore, we present some examples how modeling of pathologies is done and what kind of influence it has on cellular electrophysiology and excitation propagation. The results of these modeling studies can be used to cross-validate measurement results or to test hypotheses.

7.1 Remodeling

The effects of sustained AF can be e.g. severe congestive heart failure, thromboembolism, cardiomyopathy, ventricular arrhythmia and remodeling of the atria. This remodeling can be electrical, structural and contractile [162]. Electrical remodeling leads to a reduced APD due to a calcium overload compensation mechanism. The structural remodeling mainly reduces the CV. Both of these remodeling effects lead to a reduced wavelength favoring the continuation of AF. Contractile remodeling reduces the active tension development in atrial cells. Schotten et al. presented recently a comprehensive review article about underlying mechanisms of AF [215]. The reduction of APD is based on an increase of I_{K1} by around 110 % and a decrease of both $I_{Ca,L}$ and I_{to} by around 65 %. The structural remodeling decreases gap junction density reducing the intracellular conductivity by up to 30 %.

These values for changed atrial electrophysiology were implemented by several modeling groups, e.g. [218, 236, 267], to investigate the effects of remodeling on atrial electrophysiology, excitation propagation and vulnerability. As an example, the Courtemanche model in conjunction with the monodomain model was used to reconstruct the remodeling effects and simulate re-entry mechanisms in a schematic 2D model [218]. Both electrophysiological and structural remodeling was implemented based on literature values. The APD in tissue was reduced from 322 ms in the control case to 144 ms under remodeling. The CV was decreased from 71.5 cm/s in the physiological case to 54 cm/s. The tissue simulation showed that re-entrant patterns can be generated only for the case of remodeling and cannot be sustained in the normal atrial tissue.

7.2 Fibrosis

Atrial fibrosis increases with age and develops in conjunction with cardiomyopathy and heart failure. Fibrosis has been linked to an increased probability of arrhythmias, including AF [117]. Fibrosis is characterized by both an expansion of the extracellular space and an increase in the number of cardiac fibroblasts. The increase in extracellular

matrix reduces the conduction but only little is known about fibroblasts. As fibroblasts have mostly passive electrophysiological properties but can express functional gap junctions with myocytes, conduction can also be altered by fibroblasts [117].

Several modeling studies illustrated the impact of fibrosis on atrial electrophysiology and conduction as well as on ECGs [96, 147, 178]. Plank et al. [178] showed in a realistic atrial anatomy that increased anisotropy in the atria due to fibrosis can be responsible for the breakup of PV ectopic waves into multiple re-entrant circuits. Maleckar et al. [147] coupled a human atrial myocyte to a variable number of fibroblasts and investigated the effect of altering the intercellular coupling conductance, electrophysiological fibroblast properties, and stimulation rate on the atrial AP. The results demonstrate that the myocyte resting potential and AP waveform are modulated strongly by the properties and number of coupled fibroblasts, the degree of coupling, and the pacing frequency. Jacquemet et al. developed a 2D model of atrial tissue including microfibrosis incorporated as a set of collagenous septa disconnecting transverse coupling [96]. The density and length of these septa were varied. The analysis of unipolar electrograms showed that the septa decreased CV by up to 75% and increased the amount of fractionation and asymmetry of the electrograms.

7.3 Effects of vagal activity

Vagal nerve stimulation releases acetylcholine (ACh) as a transmitter to the whole atrium. The main effect of ACh is to slow down heart rate by decreasing the SN activity. Furthermore, ACh-dependent potassium channels also exist in atrial working myocardium. If ACh is released, the APD shortens. As the ACh release was measured to be inhomogeneous [114], APD differences can exist throughout the atrium due to vagal stimulation.

Kneller et al. [114] combined their measurements with a computational study to investigate the arrhythmogenic effects of these ACh-induced inhomogeneities of the APD. A 2D patch including periodic changes in ACh concentration was used to investigate the effects of vagal stimulation on the reentrant properties. It was found that one initial stable rotor can breakup into three re-entries under influence of ACh because the heterogeneity of refractoriness generates inhomogeneous wavefront-waveback interactions. Thereby, the model was able to support the hypothesis that vagal stimulation can have an effect on arrhythmia generation.

7.4 Pathological dilation of the atrium

Stretch-activated channels might play a role in the initiation and continuation of AF [270]. Under pathological condition, the atrium can be dilated and therefore be under a constant stretch.

Two modeling approaches have shown the potential impact of dilation to the initiation and perpetuation of AF [127, 198]. Ruiz-Villa et al. [198] showed that the vulnerability to ectopic beats is higher using a dilation model than a purely electrophysiological remodeling approach. Three different ectopic beat locations were investigated and the resulting arrhythmia properties corresponded well to measured data. Kuijpers et al. [127] simulated acute atrial dilation by increasing stretch throughout the atrial wall. This stretch was heterogeneously distributed because of geometrical effects and resulted in a higher dispersion of ERP, a slowing of conduction and local conduction block through stretch-activated currents. All these factors were shown to favor the existence of AF.

7.5 Genetic defects

Additional to other initiating factors, AF has been shown to be a heritable disorder. Recent studies have identified several genetic defects affecting atrial ion channels (e.g. [25, 155]). Chen et al. [25] studied a family with persistent AF. The family had a mutation (S140G) in the *KCNQ1* gene, which forms the α-subunit of the I_{Ks} channel. The mutation caused a gain-of-function effect, an instantaneous activation and deactivation as well as an almost linear current–voltage relationship. McPate et al. [155] measured the properties of the mutation N588K in the gene *KCNH2*, which encodes the hERG protein. This protein forms the α-subunit of the I_{Kr} channel. This mutation also causes a gain-of-function effect.

For both mutations, a computational equivalent was developed based on the Courtemanche model [217, 220]. To this end, the model parameters were adjusted to the measured voltage-clamp data defining the difference between measured and simulated ion current response to voltage steps and minimizing this difference. In case of the I_{Ks} mutation it was shown that APD_{90} was reduced to 35 % of the physiological value leading to a significant decrease in wavelength [220]. The I_{Kr} channel mutation also showed a reduction in APD (62 %) [217]. Interesting here was that the ERP in tissue showed a less pronounced reduction (27 %) as it depended on the maximum upstroke reached during depolarization leading to a less-pronounced increase of the mutant I_{Kr} in tissue compared to single cell. Nevertheless, the wavelength was also in this case reduced building a substrate for AF.

8 Towards clinical applications

The usage of atrial models has various faces. In the previous section, research applications of atrial models were presented, which help to gain a better understanding of

atrial pathologies. Another potential field of application is the usage of atrial models for a more therapy-oriented clinical research. In future, a goal could be to use computational models in clinical practice, as part of the therapy planning procedure. This section gives four examples for atrial modeling moving towards clinical application.

8.1 Improving RF ablation

Patients suffering from paroxysmal AF can be treated conventionally by drugs which suppress the symptoms of AF. Another option is the curative RF ablation therapy [20]. The minimally invasive ablation procedure was preceded by surgical procedures, such as the MAZE I–III. Although more frequently undertaken in the recent years, the success rate of ablation procedures is still variable and may differ between clinical centers and medical practitioners. Although for atrial flutter and paroxysmal AF high success rates are achieved, success rates for persistent AF are significantly smaller [20].

The treatment of AF with ablation is reviewed in Ref. [20]. Reviews about the biophysics of lesion formation during RF ablation can be found elsewhere [72, 73, 164] and modeling of the creation of a RF ablation lesion is subject to thermodynamical modeling [12].

8.1.1 Ablation lesion pattern models

Atrial models were used to find the best possible surgical pattern [196, 197, 234] and to evaluate different idealized ablation patterns on their ability to terminate AF [37, 54, 188, 195]. Some of these studies also introduced incomplete lesions to test the impact on AF recurrence [37, 188, 195, 196].

8.1.2 Simulation of gaps in RF lesions

Small gaps in ablation lesions show an isthmus-like conduction behavior. Cabo et al. [17] were able to show such slow conduction in lesion gaps both experimentally and in silico. They also discovered a distinct wave-front curvature caused by the isthmus in the lesion. Thomas et al. [231] found the behavior to depend on the size of the gap, which was confirmed recently in a combined measurement and simulation study [187]. Perez et al. [176] showed experimental evidence that conduction through discontinuities in ablation lesions is associated with gap geometry. Pop et al. [182] simulated the influence of conductivity and fiber orientation on the conduction through a gap between two scars in ventricular myocardium. Ranjan et al. [187] were also able to show a conductivity-dependent conduction behavior in silico.

8.1.3 Ablation lesions from LE-MRI

Late enhancement MRI (LE-MRI) using contrast agents provides a tool to image myocardium with reduced perfusion. Several groups have shown to image pathological regions prior to RFA [170] as well as acute and chronic scars after RFA [8, 116].

MacLeod et al. [146] highlighted the importance to include such information about structural changes of the atrial myocardium into geometrical models. Recently, first approaches have been undertaken to use patient-specific atrial models to evaluate and predict the outcome of RF ablation procedures in silico using information from LE-MRI [226]. An example for such an attempt can be seen in Fig. 6.

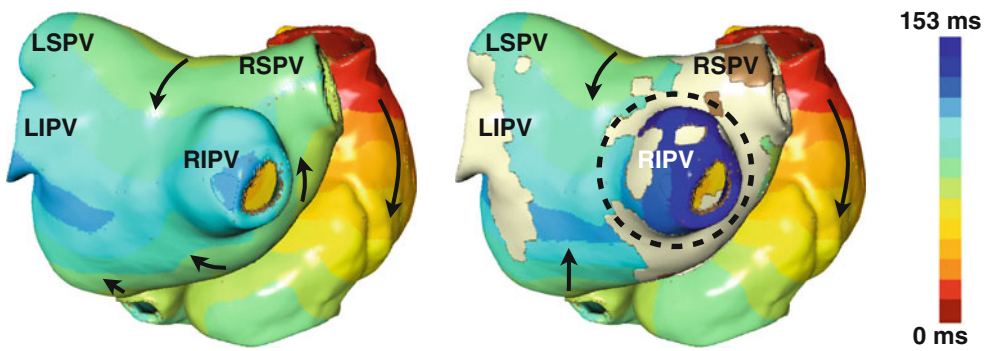

Fig. 6 Local activation times in a patient-specific model. *Left* Regular model. *Right* Model with ablation lesions derived from the same patient using LE-MRI. Data presented in Ref. [226]. Right inferior pulmonary vein is not completely isolated (*encircled*), whereas the right superior pulmonary vein is completely isolated from left atrial tissue. Activation pattern of the left atrium changes after ablation, as activation over the upper and middle posterior interatrial bridges cannot propagate any further due to the ablation lesion

8.2 Hemodialysis

End-stage renal disease patients show a higher prevalence for suffering from AF [64]. Hemodialysis therapy compensates for loss of renal function, but also alters the concentrations of blood electrolytes. A hemodialysis session lasts for several hours, so it is reasonable to assume that with the blood electrolyte also the extracellular ion concentration in the cardiac tissue will change. It was shown that alterations in electrolyte concentrations before and after a hemodialysis session impact atrial electrophysiology, slow down excitation propagation, decrease WL and prolong the P-wave both in simulations and measurements [125, 221]. The modeling approach was thereby able to close the gap in the chain of evidence between single cell measurements and body surface ECG measurements and supported the explanation of the potential risk of pro-arrhythmic effects during hemodialysis therapy. In the future, the model could be used to find the appropriate dialysis solution to minimize the risk of developing AF.

8.3 Development of signal analysis techniques

Besides the presented applications to clinical research, atrial models bear the potential as development tool for improving signal analysis and measurement techniques. To validate such techniques, they can be tested in silico in a controlled environment with no unknown variables. Especially, the quantity or property to determine is well-defined in the model. Such a validation may be used to estimate possible errors, or improve the system before any clinical studies or animal experiments are carried out.

On a single-electrogram level, it was studied how intracardiac electrogram morphology depended on the angle of the catheter tip with respect to the myocardium. To this end, different orientations were simulated using the bidomain equations and compared to clinical measurements [181]. In an arrhythmia simulation with stable rotors and multiple wavebreaks, simulated electrograms, e.g. at the rotor tip, were compared to clinical complex fractionated atrial electrogram (CFAE) signals [163].

In the context of catheter activation patterns, atrial simulations were used to develop methods to quantitatively analyze intracardiac electrogram recordings from multispline catheters [153] and circular mapping catheters [255–257]. Richter et al. [189] validated a propagation pattern analysis for AF signals in two simulation scenarios before applying it to clinical data. A method for interpolating local activation times on the complete atria from sparse measurement data with the help of a simulation model was presented for a simulated case of typical atrial flutter [139].

With respect to AF cycle length, Haissaguerre et al. demonstrated in 3D atrial simulations that the AF cycle length was inversely related to the number of active trigger sources, and then applied the cycle length analysis to clinical data [76]. Sassi et al. [210] used simulated atrial ECGs to validate methods for determining the dominant AF frequency from the T-Q interval, i.e. without removing the ventricular signal.

8.4 Atrial overdrive pacing

Besides pharmaceutical management, AF can also be terminated electrically using cardioversion or antitachycardia pacing [115], so-called overdrive pacing. External pacing with a frequency higher than the tachycardia frequency will override the tachycardia, as the stimulation introduces refractoriness in areas that previously conducted the tachycardia. Success rates are variable, and computer models bear the potential to provide a better understanding of the mechanisms of overdrive pacing and may allow an optimization of the therapy. For example, simulation results of a whole heart revealed that atrial tissue properties such as CV and APD determine the response to the therapy [244, 245]. Atrial models could therefore in future be used to determine the proper pacing site and pacing cycle length [245, 246]. Low-energy pacing can establish intramural wave sources at heterogeneities in the fibrillatory substrate and thus directly target cores of the electrical turbulences [145]. Fenton et al. [58] were able to provide a better understanding of the formation of virtual electrodes due to pulsed far-field stimulation in a combined simulation and measurement study.

9 Perspectives

Although this review article illustrates the advances that have been made in the last years in the field of atrial modeling, it is obvious that we have not yet progressed far enough to enable the simple use of the models in all areas of research and clinical application. In the following, some emergent aspects are highlighted which need further focus in future.

9.1 Computer modeling for basic research

A better understanding of initiation and perpetuation of AF is a major issue of current research. We do not yet clearly know what type of changes appear in the atrial tissue before atrial flutter and AF emerge. It becomes evident that many different processes are responsible for AF and in different patients different aspects are dominant. Computer modeling of pathological atria will contribute to the answer

of many open questions. Altered heterogeneities and anisotropies of atrial tissue promote AF and they have to be included into modeling as realistically as possible. In particular, modeling atrial tissue on cellular level including extracellular matrix (collagen) and fibroblasts will play an important role, e.g. in highlighting the origin and characteristics of CFAEs and their correlation with fibrotic tissue. Furthermore, computational modeling can help to understand atrial remodeling and the slow process of reverse remodeling after a therapeutic intervention.

9.2 Integrating elastomechanics and flow

Modeling the ventricles is in the leading edge in terms of elastomechanics and flow, probably because the fiber orientation is known better and the walls are much thicker and thus easier to model. First attempts to model the elastomechanics of the atria have been published without any link to electrophysiology [41, 101]. By integrating elastomechanics and flow into the atrial model, the filling of the ventricles with blood can be investigated and the risk for clots leading to stroke for patients suffering from AF can be estimated. Also structural remodeling, e.g. as a consequence of hypertension or persistent AF, can be investigated with the support of elastomechanical modeling.

9.3 Personalization

A fast way to build computational models of the atria of an individual patient has to be found. A versatile clinical workflow has to be implemented that includes all measurements that are essential and only adds more diagnostic procedures if unavoidable. This chain will start with improved imaging techniques [150], move on with new segmentation tools, include BSPM and end with catheter-based measurements like electrograms with specific stimulation protocols. Modeling would have an important impact, if it could lead to significantly higher therapeutic success rates in particular in case of ablation of persistent AF. However, modeling will only be accepted in clinical practice, if the price is not a longer therapeutic procedure. Presumably, patients will be sorted into groups that fit best to their specific problem and treated along a new set of group-specific clinical pathways. Algorithms to adapt model parameters to patient data have to be improved [122, 139].

9.4 Electrocardiographic imaging (ECGI)

Solving the inverse problem of electrocardiology can produce images of electrophysiology like e.g. localization of ectopic foci, activation time maps, spatially resolved CV, and visualization of fibrotic regions. The method is completely non-invasive, only a BSPM and an MRI thorax scan are needed. Unfortunately, the inverse problem is severely ill-posed in particular in the atria as the signal is lower than in the ventricles and the atria are more distant from the body surface. Promising preliminary results [34] have to be validated and new methods of regularization have to be discovered before ECGI can be used for parametrization of individual atrial models.

9.5 Drug research

The idea to support pharmacological research with computational modeling is appealing [167, 192]. Today, we encounter several problems e.g. that antiarrhythmic drugs most often change the properties of several ion channels and that the data needed for computational modeling may not be available. Nevertheless, first efforts have been undertaken to model drug effects in the atria [5, 204]. Specific information about the genetic profile of the patient can or must be included in the long run if the best drug is to be selected for an individual patient.

9.6 Ablation therapy planning

Today, generalized approaches to validate the success chance of various ablation lines using computational models have been presented. The future will be an individualized planning of ablation lines. In silico modeling of the atria must be reduced to the most essential parts since it must deliver a reliable result in real-time. Important information delivered by the models can only have impact in the EP-lab when the cardiologist gets the answer to some crucial question within a few minutes. Measurements of intraatrial electrograms with multielectrode catheters must find a straightforward way into the personalization of the model. Also ablation lines that have already been realized must be considered in the model immediately. If patients can be grouped into typical cases, e.g. using ECGI, these calculations can be done beforehand and only the case that fits best to the patient has to be selected in the EP-lab.

9.7 Prevention from atrial arrhythmias

A completely new aspect of computational modeling can be the prevention from AF. With modeling, we might be able to identify new biomarkers on different levels e.g. proteins, cell and tissue properties and in the BSPM of persons that show an increased risk for AF. In addition, specific drugs can be designed to hinder the onset of AF for those persons. Also, the models in combination with measurement studies can give hints to high risk people how to change their way of life, so that AF will not establish.

9.8 Merging imaging, electrophysiology and genomics

The authors of this review are convinced that on the long run computational modeling will be the best and may be even the only way to merge the information from imaging, electrophysiology and genomics so that all this information can be used in an optimal way for diagnosis and therapy planning.

10 Conclusion

This review has demonstrated that tremendous progress has been made in the last 10 years in modeling human atria. The contributions to research and comprehension of physiology and pathophysiology are obvious. The impact on clinical procedures is not yet as strong as envisaged. Pathologies of the atria are much more complex than expected by modeling experts. More and precise measurements on human atria are urgently needed. These data can help to select which of the currently available five cellular models fits best to reality and which one reproduces most accurately e.g. heterogeneity, restitution curves and remodeling. We need to learn how we have to model excitation propagation, so that we can replicate the real physiological and pathological case, e.g. fibrotic tissue. The community of computational modeling of the atria is encouraged to build a much stronger link to real measured data. Virtual atria with no reference to real measurements are of limited clinical use. However, continuously merging computational models with experimental and clinical data will significantly impact on a better comprehension, detailed diagnosis and a better therapy of atrial diseases.

Acknowledgments The research leading to these results has received funding from the European Community's Seventh Framework Programme (FP7/2007-2013) under grant agreement no. 224495 (euHeart project). The work of M. Wilhelms was supported by the German Research Foundation under Grant DFG SE 1758/3-1.

References

1. Al Abed A, Guo T, Lovell N, Dokos S (2010) An anatomically realistic 3d model of atrial propagation based on experimentally recorded action potentials. In: Engineering in Medicine and Biology Society (EMBC) 2010 Annual International Conference of the IEEE, pp 243–246
2. Aliot E, Haissaguerre M, Jackman W (2008) Catheter ablation of atrial fibrillation. Blackwell, USA
3. Anderson RH, Cook AC (2007) The structure and components of the atrial chambers. Europace 9(Suppl 6):3–9
4. Arora R, Verheule S, Scott L, Navarrete A, Katari V, Wilson E, Vaz D, Olgin JE (2003) Arrhythmogenic substrate of the pulmonary veins assessed by high-resolution optical mapping. Circulation 107:1816–1821
5. Aslanidi OV, Al-Owais M, Benson AP, Colman M, Garratt CJ, Gilbert SH, Greenwood JP, Holden AV, Kharche S, Kinnell E, Pervolaraki E, Plein S, Stott J, Zhang H (2011) Virtual tissue engineering of the human atrium: modelling pharmacological actions on atrial arrhythmogenesis. Eur J Pharm Sci 46(4):209–221
6. Aslanidi OV, Colman MA, Stott J, Dobrzynski H, Boyett MR, Holden AV, Zhang H (2011) 3D virtual human atria: a computational platform for studying clinical atrial fibrillation. Prog Biophys Mol Biol 107:156–168
7. Backhaus M, Britten R, Do Chung J, Cowan B, Fonseca C, Medrano-Gracia P, Tao W, Young A (2010) The cardiac atlas project: development of a framework integrating cardiac images and models. In: Camara O, Pop M, Rhode K, Sermesant M, Smith N, Young A (eds) Statistical atlases and computational models of the heart. Lecture notes in computer science, vol 6364, pp 54–64, Springer, Berlin
8. Badger TJ, Oakes RS, Daccarett M, Burgon NS, Akoum N, Fish EN, Blauer JJE, Rao SN, Adjei-Poku Y, Kholmovski EG, Vijayakumar S, Di Bella EVR, MacLeod RS, Marrouche NF (2009) Temporal left atrial lesion formation after ablation of atrial fibrillation. Heart Rhythm 6:161–168
9. Barnette AR, Bayly PV, Zhang S, Walcott GP, Ideker RE, Smith WM (2000) Estimation of 3-D conduction velocity vector fields from cardiac mapping data. IEEE Trans Biomed Eng 47: 1027–1035
10. Bayly PV, KenKnight BH, Rogers JM, Hillsley RE, Ideker RE, Smith WM (1998) Estimation of conduction velocity vector fields from epicardial mapping data. IEEE Trans Biomed Eng 45: 563–571
11. Beeler GW, Reuter H (1977) Reconstruction of the action potential of ventricular myocardial fibers. J Physiol 268:177–210
12. Berjano EJ (2006) Theoretical modeling for radiofrequency ablation: state-of-the-art and challenges for the future. Biomed Eng Online 5:24
13. Betts TR, Ho SY, Sanchez-Quintana D, Roberts PR, Anderson RH, Morgan JM (2002) Three-dimensional mapping of right atrial activation during sinus rhythm and its relationship to endocardial architecture. J Cardiovasc Electrophysiol 13:1152–1159
14. Blanc O, Virag N, Vesin JM, Kappenberger L (2001) A computer model of human atria with reasonable computation load and realistic anatomical properties. IEEE Trans Biomed Eng 48:1229–1237
15. Boineau JP, Canavan TE, Schuessler RB, Cain ME, Corr PB, Cox JL (1988) Demonstration of a widely distributed atrial pacemaker complex in the human heart. Circulation 77:1221–1237
16. Burdumy M, Luik A, Neher P, Hanna R, Krueger MW, Schilling C, Barschdorf H, Lorenz C, Seemann G, Schmitt C, Dössel O, Weber FM (2012) Comparing measured and simulated wave directions in the left atrium - a workflow for model personalization and validation. Biomed Tech (Berl) 57:79–87
17. Cabo C, Pertsov AM, Baxter WT, Davidenko JM, Gray RA, Jalife J (1994) Wave-front curvature as a cause of slow conduction and block in isolated cardiac muscle. Circ Res 75:1014–1028
18. Cabrera JA, Ho SY, Climent V, Sanchez-Quintana D (2008) The architecture of the left lateral atrial wall: a particular anatomic region with implications for ablation of atrial fibrillation. Eur Heart J 29:356–362
19. Cabrera JA, Sanchez-Quintana D, Farre J, Rubio JM, Ho SY (2005) The inferior right atrial isthmus: further architectural insights for current and coming ablation technologies. J Cardiovasc Electrophysiol 16:402–408
20. Calkins H, Brugada J, Packer DL, Cappato R, Chen SA, Crijns HJG, Damiano RJJ, Davies DW, Haines DE, Haissaguerre M,

Iesaka Y, Jackman W, Jais P, Kottkamp H, Kuck KH, Lindsay BD, Marchlinski FE, McCarthy PM, Mont JL, Morady F, Nademanee K, Natale A, Pappone C, Prystowsky E, Raviele A, Ruskin JN, Shemin RJ, Society of Thoracic Surgeons (2007) HRS/EHRA/ECAS expert consensus statement on catheter and surgical ablation of atrial fibrillation: recommendations for personnel, policy, procedures and follow-up. a report of the Heart Rhythm Society (HRS) Task Force on Catheter and Surgical Ablation of Atrial Fibrillation developed in partnership with the European Heart Rhythm Association (EHRA) and the European Cardiac Arrhythmia Society (ECAS); in collaboration with the American College of Cardiology (ACC), American Heart Association (AHA), and the Society of Thoracic Surgeons (STS). endorsed and approved by the governing bodies of the American College of Cardiology, the American Heart Association, the European Cardiac Arrhythmia Society, the European Heart Rhythm Association, the Society of Thoracic Surgeons, and the Heart Rhythm Society

21. Calkins H, Ho SY, Angel Cabrera J, Della Bella P, Farre J, Kautzner J, Tchou P (2008) Anatomy of the left atrium and pulmonary veins. International Journal of Cardiology, Blackwell, USA, pp 1–10
22. Campos FO, Wiener T, Prassl AJ, Ahammer H, Plank G, Weber Dos Santos R, Sanchez-Quintana D, Hofer E (2010) A 2D-computer model of atrial tissue based on histographs describes the electro-anatomical impact of microstructure on endocardiac potentials and electric near-fields. In: Engineering in medicine and biology society (EMBC), 2010 Annual international conference of the IEEE, pp 2541–2544
23. Chandler NJ, Greener ID, Tellez JO, Inada S, Musa H, Molenaar P, Difrancesco D, Baruscotti M, Longhi R, Anderson RH, Billeter R, Sharma V, Sigg DC, Boyett MR, Dobrzynski H (2009) Molecular architecture of the human sinus node: insights into the function of the cardiac pacemaker. Circulation 119:1562–1575
24. Chen SA, Hsieh MH, Tai CT, Tsai CF, Prakash VS, Yu WC, Hsu TL, Ding YA, Chang MS (1999) Initiation of atrial fibrillation by ectopic beats originating from the pulmonary veins: electrophysiological characteristics, pharmacological responses, and effects of radiofrequency ablation. Circulation 100:1879–1886
25. Chen YH, Xu SJ, Bendahhou S, Wang XL, Wang Y, Xu WY, Jin HW, Sun H, Su XY, Zhuang QN, Yang YQ, Li YB, Liu Y, Xu HJ, Li XF, Ma N, Mou CP, Chen Z, Barhanin J, Huang W (2003) KCNQ1 gain-of-function mutation in familial atrial fibrillation. Science 299:251–254
26. Cherry EM, Fenton FH (2008) Visualization of spiral and scroll waves in simulated and experimental cardiac tissue. New J Phys 10:125016
27. Cherry EM, Hastings HM, Evans SJ (2008) Dynamics of human atrial cell models: restitution, memory, and intracellular calcium dynamics in single cells. Prog Biophys Mol Biol 98:24–37
28. Clavier L, Boucher JM, Lepage R, Blanc JJ, Cornily JC (2002) Automatic P-wave analysis of patients prone to atrial fibrillation. Med Biol Eng Comput 40:63–71
29. Clayton RH, Bernus O, Cherry EM, Dierckx H, Fenton FH, Mirabella L, Panfilov AV, Sachse FB, Seemann G, Zhang H (2011) Models of cardiac tissue electrophysiology: progress, challenges and open questions. Prog Biophys Mol Biol 104:22–48
30. Coffey JL, Cristy M, Warner GG (1981) Specific absorbed fractions for photon sources uniformly distributed in the heart chambers and heart wall of a heterogeneous phantom. J Nucl Med 22:65–71
31. Courtemanche M, Ramirez RJ, Nattel S (1998) Ionic mechanisms underlying human atrial action potential properties: Insights from a mathematical model. Am J Physiol 275:H301–H321
32. Courtemanche M, Ramirez RJ, Nattel S (1999) Ionic targets for drug therapy and atrial fibrillation-induced electrical remodeling: insights from a mathematical model. Cardiovasc Res 42:477–489
33. Cristoforetti A, Masè M, Ravelli F (2010) A computationally efficient patient-specific simulation model for the investigation of arrhythmia mechanisms. In: Proceedings of ICE 2010, p 142
34. Cuculich PS, Wang Y, Lindsay BD, Faddis MN, Schuessler RB, Damiano RJ, Li L, Rudy Y (2010) Noninvasive characterization of epicardial activation in humans with diverse atrial fibrillation patterns. Circulation 122:1364–1372
35. van Dam PM, van Oosterom A (2003) Atrial excitation assuming uniform propagation. J Cardiovasc Electrophysiol 14:S166–S171
36. van Dam PM, van Oosterom A (2005) Volume conductor effects involved in the genesis of the P wave. Europace 7(Suppl 2):30–38
37. Dang L, Virag N, Ihara Z, Jacquemet V, Vesin JM, Schlaepfer J, Ruchat P, Kappenberger L (2005) Evaluation of ablation patterns using a biophysical model of atrial fibrillation. Ann Biomed Eng 33:465–474
38. De Ponti R, Ho SY, Salerno-Uriarte JA, Tritto M, Spadacini G (2002) Electroanatomic analysis of sinus impulse propagation in normal human atria. J Cardiovasc Electrophysiol 13:1–10
39. De Sisti A, Leclercq JF, Stiubei M, Fiorello P, Halimi F, Attuel P (2002) P wave duration and morphology predict atrial fibrillation recurrence in patients with sinus node dysfunction and atrial-based pacemaker. Pacing Clin Electrophysiol 25:1546–1554
40. Deneke T, Khargi K, Muller KM, Lemke B, Mugge A, Laczkovics A, Becker AE, Grewe PH (2005) Histopathology of intraoperatively induced linear radiofrequency ablation lesions in patients with chronic atrial fibrillation. Eur Heart J 26:1797–1803
41. Di Martino ES, Bellini C, Schwartzman DS (2011) In vivo porcine left atrial wall stress: computational model. J Biomech 44:2589–2594
42. Dierckx H, Bernus O, Verschelde H (2011) Accurate eikonal-curvature relation for wave fronts in locally anisotropic reaction-diffusion systems. Phys Rev Lett 107:108101
43. Dierckx H, Cherry E, Bernus O, Gilbert S, Holden A, Gilmour RFJ, Fenton FF (2008) Detailed anatomical reconstruction of the whole canine heart including fiber and sheet architecture using MRI and DTMRI. Heart Rhythm 5:106
44. Dilaveris PE, Gialafos EJ, Sideris SK, Theopistou AM, Andrikopoulos GK, Kyriakidis M, Gialafos JE, Toutouzas PK (1998) Simple electrocardiographic markers for the prediction of paroxysmal idiopathic atrial fibrillation. Am Heart J 135:733–738
45. Dimitri H, Ng M, Brooks AG, Kuklik P, Stiles MK, Lau DH, Antic N, Thornton A, Saint DA, McEvoy D, Antic R, Kalman JM, Sanders P (2012) Atrial remodeling in obstructive sleep apnea: implications for atrial fibrillation. Heart Rhythm 9(3):321–327
46. Dokos S, Cloherty SL, Lovell NH (2007) Computational model of atrial electrical activation and propagation. In: Engineering in medicine and biology society (EMBC), 2007 Annual international conference of the IEEE, vol 2007, pp 908–911
47. Dong J, Dalal D, Scherr D, Cheema A, Nazarian S, Bilchick K, Almasry I, Cheng A, Henrikson CA, Spragg D, Marine JE, Berger RD, Calkins H (2007) Impact of heart rhythm status on registration accuracy of the left atrium for catheter ablation of atrial fibrillation. J Cardiovasc Electrophysiol 18:1269–1276
48. Dössel O, Krueger MW, Weber FM, Schilling C, Schulze WHW, Seemann G (2011) A framework for personalization of computational models of the human atria. In: Proceedings of

IEEE conference IEEE Engineering, Medical Biological Society 2011, pp 4324–4328
49. Ecabert O, Peters J, Schramm H, Lorenz C, von Berg J, Walker MJ, Vembar M, Olszewski ME, Subramanyan K, Lavi G, Weese J (2008) Automatic model-based segmentation of the heart in CT images. IEEE Trans Med Imag 27:1189–1201
50. Ecabert O, Peters J, Walker MJ, Ivanc T, Lorenz C, von Berg J, Lessick J, Vembar M, Weese J (2011) Segmentation of the heart and great vessels in CT images using a model-based adaptation framework. Med Image Anal 15:863–876
51. Efimov IR, Nikolski VP, Bub G (2004) Optical mapping. In: Wenk GE et al (eds) Encyclopedia of biomaterials and biomedical engineering. Marcel Dekker, New York, pp 1133–1142
52. Efimov IR, Nikolski VP, Salama G (2004) Optical imaging of the heart. Circ Res 95:21–33
53. Ellis WS, SippensGroenewegen A, Auslander DM, Lesh MD (2000) The role of the crista terminalis in atrial flutter and fibrillation: a computer modeling study. Ann Biomed Eng 28:742–754
54. Ellis WS, SippensGroenewegen A, Lesh MD (1997) The effect of linear lesions on atrial defibrillation threshold and spontaneous termination. A computer modeling study. Pacing Clin Electrophysiol 20:1145
55. Feld GK, Mollerus M, Birgersdotter-Green U, Fujimura O, Bahnson TD, Boyce K, Rahme M (1997) Conduction velocity in the tricuspid valve-inferior vena cava isthmus is slower in patients with type I atrial flutter compared to those without a history of atrial flutter. J Cardiovasc Electrophysiol 8:1338–1348
56. Feng J, Yue L, Wang Z, Nattel S (1998) Ionic mechanisms of regional action potential heterogeneity in the canine right atrium. Circ Res 83:541–551
57. Fenton F, Karma A (1998) Vortex dynamics in three-dimensional continuous myocardium with fiber rotation: filament instability and fibrillation. Chaos 8:20–27
58. Fenton FH, Luther S, Cherry EM, Otani NF, Krinsky V, Pumir A, Bodenschatz E, Gilmour RFJ (2009) Termination of atrial fibrillation using pulsed low-energy far-field stimulation. Circulation 120:467–476
59. Fink M, Niederer SA, Cherry EM, Fenton FH, Koivumäki JT, Seemann G, Thul R, Zhang H, Sachse FB, Beard D, Crampin EJ, Smith NP (2011) Cardiac cell modelling: observations from the heart of the cardiac physiome project. Prog Biophys Mol Biol 104:2–21
60. Fitzgerald TN, Brooks DH, Triedman JK (2005) Identification of cardiac rhythm features by mathematical analysis of vector fields. IEEE Trans Biomed Eng 52:19–29
61. FitzHugh RA (1961) Impulses and physiological states in theoretical models of nerve membran. Biophys J 1:445–466
62. Freudenberg J, Schiemann T, Tiede U, Hohne KH (2000) Simulation of cardiac excitation patterns in a three-dimensional anatomical heart atlas. Comput Biol Med 30:191–205
63. Fuster V, Ryden LE, Cannom DS, Crijns HJ, Curtis AB, Ellenbogen KA, Halperin JL, Le Heuzey JY, Kay GN, Lowe JE, Olsson SB, Prystowsky EN, Tamargo JL, Wann S, Smith SCJ, Jacobs AK, Adams CD, Anderson JL, Antman EM, Hunt SA, Nishimura R, Ornato JP, Page RL, Riegel B, Priori SG, Blanc JJ, Budaj A, Camm AJ, Dean V, Deckers JW, Despres C, Dickstein K, Lekakis J, McGregor K, Metra M, Morais J, Osterspey A, Zamorano JL, Heart Rhythm Society (2006) ACC/AHA/ESC 2006 guidelines for the management of patients with atrial fibrillation: a report of the American College of Cardiology/American Heart Association Task Force on Practice Guidelines and the European Society of Cardiology Committee for Practice Guidelines (Writing Committee to Revise the 2001 Guidelines for the Management of Patients With Atrial Fibrillation): developed in collaboration with the European Heart Rhythm Association and the Heart Rhythm Society
64. Genovesi S, Vincenti A, Rossi E, Pogliani D, Acquistapace I, Stella A, Valsecchi MG (2008) Atrial fibrillation and morbidity and mortality in a cohort of long-term hemodialysis patients. Am J Kidney Dis 51:255–262
65. Gianni D, McKeever S, Yu T, Britten R, Delingette H, Frangi A, Hunter P, Smith N (2010) Sharing and reusing cardiovascular anatomical models over the web: a step towards the implementation of the virtual physiological human project. Philos Trans A Math Phys Eng Sci 368:3039–3056
66. Gong Y, Xie F, Stein KM, Garfinkel A, Culianu CA, Lerman BB, Christini DJ (2007) Mechanism underlying initiation of paroxysmal atrial flutter/atrial fibrillation by ectopic foci: a simulation study. Circulation 115:2094–2102
67. Gozolits S, Fischer G, Berger T, Hanser F, Abou-Harb M, Tilg B, Pachinger O, Hintringer F, Roithinger FX (2002) Global P wave duration on the 65-lead ECG: single-site and dual-site pacing in the structurally normal human atrium. J Cardiovasc Electrophysiol 13:1240–1245
68. Grandi E, Pandit SV, Voigt N, Workman AJ, Dobrev D, Jalife J, Bers DM (2011) Human atrial action potential and Ca^{2+} model: sinus rhythm and chronic atrial fibrillation. Circulation Research 109:1055–1066
69. Grandi E, Pasqualini FS, Bers DM (2010) A novel computational model of the human ventricular action potential and Ca transient. J Mol Cell Cardiol 48:112–121
70. Gray RA, Jalife J (1998) Ventricular fibrillation and atrial fibrillation are two different beasts. Chaos 8:65–78
71. Guidera SA, Steinberg JS (1993) The signal-averaged P wave duration: a rapid and noninvasive marker of risk of atrial fibrillation. J Am Coll Cardiol 21:1645–1651
72. Haemmerich D (2010) Biophysics of radiofrequency ablation. Crit Rev Biomed Eng 38:53–63
73. Haines DE (2008) Catheter ablation of cardiac arrhythmias: basic concepts and clinical applications. 3rd edn Biophysics and pathophysiology of lesion formation by transcatheter radiofrequency ablation pp. 20–34. Blackwell Futura Wiley Online Library
74. Haissaguerre M, Jais P, Shah DC, Arentz T, Kalusche D, Takahashi A, Garrigue S, Hocini M, Peng J.T, Clementy J (2000) Catheter ablation of chronic atrial fibrillation targeting the reinitiating triggers. J Cardiovasc Electrophysiol 11:2–10
75. Haissaguerre M, Jaïs P, Shah DC, Takahashi A, Hocini M, Quiniou G, Garrigue S, Le Mouroux A, Le Métayer P, Clémenty J (1998) Spontaneous initiation of atrial fibrillation by ectopic beats originating in the pulmonary veins. N Engl J Med 339:659–666
76. Haissaguerre M, Lim KT, Jacquemet V, Rotter M, Dang L, Hocini M, Matsuo S, Knecht S, Jais P, Virag N (2007) Atrial fibrillatory cycle length: computer simulation and potential clinical importance. Europace 9:vi64–vi70
77. Hall B, Jeevanantham V, Simon R, Filippone J, Vorobiof G, Daubert J (2006) Variation in left atrial transmural wall thickness at sites commonly targeted for ablation of atrial fibrillation. J Interv Card Electrophysiol 17:127–132
78. Hanna R, Barschdorf H, Klinder T, Weber FM, Krueger MW, Dössel O, Lorenz C (2011) A hybrid method for automatic anatomical variant detection and segmentation. In: Functional Imaging and Modeling of the Heart 2011 Lecture Notes in Computer Science 6666 pp 333–340
79. Hansson A, Holm M, Blomstrom P, Johansson R, Luhrs C, Brandt J, Olsson S (1998) Right atrial free wall conduction velocity and degree of anisotropy in patients with stable sinus rhythm studied during open heart surgery. Eur. Heart. J. 19:293–300

80. Harrild DM, Henriquez CS (2000) A computer model of normal conduction in the human atria. Circ Res 87:e25–e36
81. Hassink RJ, Aretz HT, Ruskin J, Keane D (2003) Morphology of atrial myocardium in human pulmonary veins: a postmortem analysis in patients with and without atrial fibrillation. J Am Coll Cardiol 42:1108–1114
82. Henriquez CS (1993) Simulating the electrical behavior of cardiac tissue using the bidomain model. Crit Rev Biomed Eng 21:1–77
83. Hermosillo BDF (2008) Semi-automatic enhancement of atrial models to include atrial architecture and patient specific data: for biophysical simulations. In: Proceedings of computers in cardiology. vol 35, pp 633–636
84. Ho SY, Anderson RH, Sánchez-Quintana D (2002) Atrial structure and fibres: morphologic bases of atrial conduction. Cardiovasc Res 54:325–336
85. Ho SY, Becker AE (2008) Anatomy of electrophysiology. In: Fuster V, Hurst JW, O'Rourke RA, Walsh RA, King SB, Poole-Wilson PA (eds) The Heart. 12th edn
86. Ho SY, Cabrera JA, Tran VH, Farre J, Anderson RH, Sanchez-Quintana D (2001) Architecture of the pulmonary veins: relevance to radiofrequency ablation. Heart 86:265–270
87. Ho SY, Sanchez-Quintana D (2008) The importance of atrial structure and fibers. Clin Anat 22:52–63
88. Ho SY, Sanchez-Quintana D, Cabrera JA, Anderson RH (1999) Anatomy of the left atrium: implications for radiofrequency ablation of atrial fibrillation. J Cardiovasc Electrophysiol 10:1525–1533
89. Hocini M, Ho SY, Kawara T, Linnenbank AC, Potse M, Shah D, Jais P, Janse MJ, Haissaguerre M, De Bakker JM (2002) Electrical conduction in canine pulmonary veins: electrophysiological and anatomic correlation. Circulation 105:2442–2448
90. Hocini M, Loh P, Ho SY, Sanchez-Quintana D, Thibault B, de Bakker JM, Janse MJ (1998) Anisotropic conduction in the triangle of Koch of mammalian hearts: electrophysiologic and anatomic correlations. J Am Coll Cardiol 31:629–636
91. Hodgkin AL, Huxley AF (1952) A quantitative description of membrane current and its application to conduction and excitation in nerve. J Physiol 117:500–544
92. Holmqvist F, Carlson J, Platonov PG (2009) Detailed ECG analysis of atrial repolarization in humans. Ann Noninvasive Electrocardiol 14:13–18
93. Holmqvist F, Husser D, Tapanainen JM, Carlson J, Jurkko R, Xia Y, Havmoller R, Kongstad O, Toivonen L, Olsson SB, Platonov PG (2008) Interatrial conduction can be ACCurately determined using standard 12-lead electrocardiography: validation of P-wave morphology using electroanatomic mapping in man. Heart Rhythm 5:413–418
94. Ionasec R, Voigt I, Mihalef V, Grbic S, Vitanovski D, Wang Y, Zheng Y, Hornegger J, Navab N, Georgescu B, Comaniciu D (2010) Patient-specific modeling of the heart: Applications to cardiovascular disease management. In: Camara O, Pop M, Rhode K Sermesant M, Smith N, Young A (eds) Statistical Atlases and Computational Models of the Heart 2010 Lecture Notes in Computer Science vol. 6364, Springer, Berlin, pp 14–24
95. Jacquemet V (2011) An eikonal-diffusion solver and its application to the interpolation and the simulation of reentrant cardiac activations. Computer Methods and Programs in Biomedicine
96. Jacquemet V, Henriquez CS (2009) Genesis of complex fractionated atrial electrograms in zones of slow conduction: a computer model of microfibrosis. Heart Rhythm 6:803–810
97. Jacquemet V, Kappenberger L, Henriquez CS (2008) Modeling atrial arrhythmias: Impact on clinical diagnosis and therapies. IEEE Rev Biomed Eng 1:94–114
98. Jacquemet V, Lemay M, van Oosterom A, Kappenberger L (2006) The equivalent dipole used to characterize atrial fibrillation. In: Proceedings of computers in cardiology. vol 33, pp 149–152, IEEE 17–20 Sept, Valencia
99. Jacquemet V, van Oosterom A, Vesin JM, Kappenberger L (2006) Analysis of electrocardiograms during atrial fibrillation. A biophysical model approach. IEEE Eng Med Biol Mag 25:79–88
100. Jacquemet V, Virag N, Ihara Z, Dang L, Blanc O, Zozor S, Vesin JM, Kappenberger L, Henriquez C (2003) Study of unipolar electrogram morphology in a computer model of atrial fibrillation. J Cardiovasc Electrophysiol 14:S172–S179
101. Jernigan SR, Buckner GD, Eischen JW, Cormier DR (2007) Finite element modeling of the left atrium to facilitate the design of an endoscopic atrial retractor. J Biomech Eng 129:825–837
102. Jongbloed MRM, Lamb HJ, Bax JJ, Schuijf JD, de Roos A, van der Wall EE, Schalij MJ (2005) Noninvasive visualization of the cardiac venous system using multislice computed tomography. J Am Coll Cardiol 45:749–753
103. Kafer CJ (1991) Internodal pathways in the human atria: a model study. Comp Biomed Res 24:549–563
104. Kalifa J, Klos M, Zlochiver S, Mironov S, Tanaka K, Ulahannan N, Yamazaki M, Jalife J, Berenfeld O (2007) Endoscopic fluorescence mapping of the left atrium: a novel experimental approach for high resolution endocardial mapping in the intact heart. Heart Rhythm 4:916–924
105. Kanagaratnam P, Rothery S, Patel P, Severs NJ, Peters, NS (2002) Relative expression of immunolocalized connexins 40 and 43 correlates with human atrial conduction properties. J Am Coll Cardiol 39:116–123
106. Kaseno K, Tada H, Koyama K, Jingu M, Hiramatsu S, Yokokawa M, Goto K, Naito S, Oshima S, Taniguchi K (2008) Prevalence and characterization of pulmonary vein variants in patients with atrial fibrillation determined using 3-dimensional computed tomography. Am J Cardiol 101:1638–1642
107. Kato R, Lickfett L, Meininger G, Dickfeld T, Wu R, Juang G, Angkeow P, LaCorte J, Bluemke D, Berger R, Halperin HR, Calkins H (2003) Pulmonary vein anatomy in patients undergoing catheter ablation of atrial fibrillation: lessons learned by use of magnetic resonance imaging. Circulation 107:2004–2010
108. Keith A, Flack MW (1907) The form and nature of the muscular connections between the primary divisions of the vertebrate heart. J Anat Physiol 41:172–189
109. Keller DUJ, Weber FM, Seemann G, Dössel O (2010) Ranking the influence of tissue conductivities on forward-calculated ECGs. IEEE Trans Biomed Eng 57:1568–1576
110. Kharche S, Seemann G, Margetts L, Leng J, Holden AV, Zhang H (2008) Simulation of clinical electrophysiology in 3D human atria: a high-performance computing and high-performance visualization application. Concurr Comput Pract Experience 20:1317–1328
111. Kim BS, Kim YH, Hwang GS, Pak HN, Lee SC, Shim, WJ, Oh DJ, Ro YM (2002) Action potential duration restitution kinetics in human atrial fibrillation. J Am Coll Cardiol 39:1329–1336
112. Kleber AG, Rudy Y (2004) Basic mechanisms of cardiac impulse propagation and associated arrhythmias. Physiol Rev 84:431–488
113. Kneller J, Ramirez RJ, Chartier D, Courtemanche M, Nattel S (2002) Time-dependent transients in an ionically based mathematical model of the canine atrial action potential. Am J Physiol Heart Circ Physiol 282:H1437–H1451
114. Kneller J, Zou R, Vigmond EJ, Wang Z, Leon LJ, Nattel S (2002) Cholinergic atrial fibrillation in a computer model of a two-dimensional sheet of canine atrial cells with realistic ionic properties. Circ Res 90:73
115. Knight BP, Gersh BJ, Carlson MD, Friedman PA, McNamara RL, Strickberger SA, Tse HF, Waldo AL (2005) Role of permanent pacing to prevent atrial fibrillation: science advisory

from the American Heart Association Council on Clinical Cardiology (Subcommittee on Electrocardiography and Arrhythmias) and the Quality of Care and Outcomes Research Interdisciplinary Working Group in collaboration with the Heart Rhythm Society. Circulation 111:240–243
116. Knowles BR, Caulfield D, Cooklin M, Rinaldi CA, Gill, J, Bostock J, Razavi R, Schaeffter T, Rhode KS (2010) 3-D visualization of acute RF ablation lesions using MRI for the simultaneous determination of the patterns of necrosis and edema. IEEE Trans Biomed Eng 57:1467–1475
117. Kohl P, Camelliti P, Burton FL, Smith GL (2005) Electrical coupling of fibroblasts and myocytes: relevance for cardiac propagation. J Electrocardiol 38:45–50
118. Kohl P, Noble D, Winslow RL, Hunter PJ (2000) Computational modelling of biological systems: tools and visions. Phil Trans R Soc Lond A 358:579–610
119. Koivumaeki JT, Korhonen T, Tavi P (2011) Impact of sarcoplasmic reticulum calcium release on calcium dynamics and action potential morphology in human atrial myocytes: a computational study. PLoS Comput Biol 7:e1001067
120. Kojodjojo P, Kanagaratnam P, Markides V, Davies DW, Peters N (2006) Age-related changes in human left and right atrial conduction. J Cardiovasc Electrophysiol 17:120–127
121. Kojodjojo P, Peters NS, Davies DW, Kanagaratnam P (2007) Characterization of the electroanatomical substrate in human atrial fibrillation: the relationship between changes in atrial volume, refractoriness, wavefront propagation velocities, and AF burden. J Cardiovasc Electrophysiol 18:269–275
122. Konukoglu E, Relan J, Cilingir U, Menze BH, Chinchapatnam P, Jadidi A, Cochet H, Hocini M, Delingette H, Jais P, Haissaguerre M, Ayache N, Sermesant M (2011) Efficient probabilistic model personalization integrating uncertainty on data and parameters: Application to eikonal-diffusion models in cardiac electrophysiology. Prog Biophys Mol Biol 107:134–146
123. Krueger MW, Rhode K, Weber FM, Keller DUJ, Caulfield D, Seemann G, Knowles BR, Razavi R, Dössel O (2010) Patient-specific volumetric atrial models with electrophysiological components: A comparison of simulations and measurements. Biomed Eng 55(s1):54–57
124. Krueger MW, Schmidt V, Tobón C, Weber FM, Lorenz, C, Keller DUJ, Barschdorf H, Burdumy M, Neher P, Plank, G, Rhode K, Seemann G, Sanchez-Quintana D, Saiz J, Razavi, R, Dössel O (2011) Modeling atrial fiber orientation in patient-specific geometries: a semi-automatic rule-based approach. In: Axel L, Metaxas D (eds) Functional Imaging and Modeling of the Heart 2011 Lecture Notes in Computer Science, vol 6666, pp 223–232
125. Krueger MW, Severi S, Rhode K, Genovesi S, Weber FM, Vincenti A, Fabbrini P, Seemann G, Razavi R, Dössel O (2011) Alterations of atrial electrophysiology related to hemodialysis session: insights from a multiscale computer model. J Electrocardiol 44:176–183
126. Krueger MW, Weber FM, Seemann G, Dössel O (2009) Semi-automatic segmentation of sinus node, Bachmann's Bundle and Terminal Crest for patient specific atrial models. In: World congress on medical physics and biomedical engineering. IFMBE Proceedings, vol 25/4, pp 673–676 Springer, Heidelberg
127. Kuijpers NHL, Potse M, van Dam PM, ten Eikelder HMM, Verheule S, Prinzen FW, Schotten U (2011) Mechanoelectrical coupling enhances initiation and affects perpetuation of atrial fibrillation during acute atrial dilation. Heart Rhythm 8:429–436
128. Kuijpers NHL, Rijken RJ, ten Eikelder HMM, Hilbers PAJ (2007) Vulnerability to atrial fibrillation under stretch can be explained by stretch-activated channels. In: Proceedings of computers in cardiology. vol 34, pp 237–240
129. Lakatta E, Maltsev V (2012) Rebuttal: what I_f the shoe doesn't fit? "The funny current has a major pacemaking role in the sinus node". Heart Rhythm 9:459–460
130. Lemery R, Guiraudon G, Veinot JP (2003) Anatomic description of Bachmann's bundle and its relation to the atrial septum. Am J Cardiol 91:1482–1485A8
131. Lemery R, Soucie L, Martin B, Tang ASL, Green M, Healey J (2004) Human study of biatrial electrical coupling: determinants of endocardial septal activation and conduction over interatrial connections. Circulation 110:2083–2089
132. Lesh MD, Kalman JM, Olgin JE, Ellis WS (1996) The role of atrial anatomy in clinical atrial arrhythmias. J Electrocardiol 29 (Suppl):101–113
133. Li D, Li CY, Yong AC, Johnston PR, Kilpatrick D (1999) Epicardial ST depression in acute myocardial infarction. Circ Res 85:959–964
134. Li D, Zhang L, Kneller J, Nattel S (2001) Potential ionic mechanism for repolarization differences between canine right and left atrium. Circ Res 88:1168–1175
135. Lian J, Li G, Cheng J, Avitall B, He B (2002) Body surface Laplacian mapping of atrial depolarization in healthy human subjects. Med Biol Eng Comput 40:650–659
136. Lin SF, Wikswo JP (1999) Panoramic optical imaging of electrical propagation in isolated heart. J Biomed Optics 4:200–207
137. Lin WS, Prakash VS, Tai CT, Hsieh MH, Tsai CF, Yu WC, Lin YK, Ding YA, Chang MS, Chen SA (2000) Pulmonary vein morphology in patients with paroxysmal atrial fibrillation initiated by ectopic beats originating from the pulmonary veins: implications for catheter ablation. Circulation 101:1274–1281
138. Lindblad DS, Murphey CR, Clark JW, Giles WR (1996) A model of the action potential and underlying membrane currents in a rabbit atrial cell. Am J Physiol 271:1666
139. Lines GT, MacLachlan MC, Linge S, Tveito A (2009) Synchronizing computer simulations with measurement data for a case of atrial flutter. Ann Biomed Eng 37:1287–1293
140. Lombaert H, Peyrat JM, Croisille P, Rapacchi S, Fanton L, Clarysse P, Delingette H, Ayache N (2011) Statistical analysis of the human cardiac fiber architecture from DT-MRI. In: D. Metaxas L. Axel (eds) Functional Imaging and Modeling of the Heart, Lecture Notes in Computer Science. vol 6666, pp 171–179, Springer, Berlin
141. Lorange M, Gulrajani RM (1993) A computer heart model incorporating anisotropic propagation. i. model construction and simulation of normal activation. J Electrocardiol 26:245–261
142. Lu W, Zhu X, Chen W, Wei D (2011) A computer model based on real anatomy for electrophysiology study. Adv Eng Softw 42:463–476
143. Luo CH, Rudy Y (1991) A model of the ventricular cardiac action potential. Depolarization repolarization and their interaction. Circ Res 68:1501–1526
144. Luo CH, Rudy Y (1994) A dynamic model of the cardiac ventricular action potential. I. Simulations of ionic currents and concentraion changes. Circ Res 74:1071–1096
145. Luther S, Fenton FH, Kornreich BG, Squires A, Bittihn P, Hornung D, Zabel M, Flanders J, Gladuli A, Campoy L, Cherry EM, Luther G, Hasenfuss G, Krinsky VI, Pumir A, Gilmour RFJ, Bodenschatz E (2011) Low-energy control of electrical turbulence in the heart. Nature 475: 235–239
146. MacLeod RS, Kholmovski E, DiBella EVR, Oakes RS, Blauer JE, Fish E, Vijayakumar S, Daccarett M, Segerson, NM, Marrouche NF (2008) Integration of MRI in evaluation and ablation of atrial fibrillation. In: Proceedings of Computers in Cardiology. vol 35, pp 77–80
147. Maleckar MM, Greenstein JL, Giles WR, Trayanova NA (2009) Electrotonic coupling between human atrial myocytes and

fibroblasts alters myocyte excitability and repolarization. Biophys J 97:2179–2190
148. Maleckar MM, Greenstein JL, Trayanova NA, Giles WR (2008) Mathematical simulations of ligand-gated and cell-type specific effects on the action potential of human atrium. Prog Biophy Mol Biol 98:161–170
149. Mansour M, Holmvang G, Sosnovik D, Migrino R, Abbara S, Ruskin J, Keane D (2004) Assessment of pulmonary vein anatomic variability by magnetic resonance imaging: implications for catheter ablation techniques for atrial fibrillation. J Cardiovasc Electrophysiol 15:387–393
150. Manzke R, Meyer C, Ecabert O, Peters J, Noordhoek NJ, Thiagalingam A, Reddy VY, Chan RC, Weese J (2010) Automatic segmentation of rotational X-ray images for anatomic intra-procedural surface generation in atrial fibrillation ablation procedures. IEEE Trans Med Imag 29:260–272
151. Markides V, Schilling RJ, Ho SY, Chow AWC, Davies DW, Peters NS (2003) Characterization of left atrial activation in the intact human heart. Circulation 107:733–739
152. Marom EM, Herndon JE, Kim YH, McAdams HP (2004) Variations in pulmonary venous drainage to the left atrium: implications for radiofrequency ablation. Radiology 230:824–829
153. Mase M, Del Greco M, Marini M, Ravelli F (2004) Velocity field analysis of activation maps in atrial fibrillation : a simulation study. In: IFMBE Proceedings world congress on medical physics and biomedical engineering, vol 25/4, pp 1014–1017
154. Mase M, Ravelli F (2010) Automatic reconstruction of activation and velocity maps from electro-anatomic data by radial basis functions. In: Engineering in Medicine and Biology Society (EMBC), 2010 Annual International Conference of the IEEE, vol 2010, pp 2608–2611
155. McPate MJ, Duncan RS, Milnes JT, Witchel HJ, Hancox JC (2005) The N588K-HERG K+ channel mutation in the "short QT syndrome": mechanism of gain-in-function determined at 37 degrees C. Biochem Biophy Res Commun 334:441–449
156. Mihalef V, Ionasec RI, Sharma P, Georgescu B, Voigt I, Suehling M, Comaniciu D (2011) Patient-specific modelling of whole heart anatomy, dynamics and haemodynamics from four-dimensional cardiac CT images. Interface Focus 1:286–296
157. Millar CK, Kralios FA, Lux RL (1985) Correlation between refractory periods and activation-recovery intervals from electrograms: effects of rate and adrenergic interventions. Circulation 72:1372–1379
158. Mirvis DM (1980) Body surface distribution of electrical potential during atrial depolarization and repolarization. Circulation 62:167–173
159. Mlcochova H, Tintera J, Porod V, Peichl P, Cihak R, Kautzner J (2005) Magnetic resonance angiography of pulmonary veins: implications for catheter ablation of atrial fibrillation. Pacing Clin Electrophysiol 28:1073–1080
160. Moe GK, Rheinboldt WC, Abildskov JA (1964) A computer model of atrial fibrillation. Am Heart J 67:200–220
161. Nathan H, Eliakim M (1966) The junction between the left atrium and the pulmonary veins. An anatomic study of human hearts. Circulation 34:412–422
162. Nattel S (2002) New ideas about atrial fibrillation 50 years on. Nature 415:219–226
163. Navoret N, Xu B, Jacquir S, Binczak S (2010) Comparison of complex fractionated atrial electrograms at cellular scale using numerical and experimental models. In: Engineering in medicine and biology society (EMBC), 2010 Annual International Conference of the IEEE, vol 2010, pp 3249–3252
164. Ndrepepa G, Estner H (2006) Ablation of cardiac arrhythmias energy sources and mechanisms of lesion formation. In: Schmitt C, Deisenhofer I, Zrenner B (eds) Catheter ablation of cardiac arrhythmias, Steinkopff, pp 35–53
165. Neher P, Barschdorf H, Dries S, Weber FM, Krueger MW, Dössel O, Lorenz C (2011) Automatic segmentation of cardiac CTs— personalized atrial models augmented with electrophysiological structures. In: Functional Imaging and Modeling of the Heart 2011 Lecture Notes in Computer Science, vol 6666, pp 80–87
166. Noble D (2002) Modeling the heart: from genes to cells to the whole organ. Science 295:1678–1682
167. Noble D (2008) Computational models of the heart and their use in assessing the actions of drugs. J Pharm Sci 107:107–117
168. Nygren A, Fiset C, Firek L, Clark JW, Lindblad DS, Clark RB, Giles WR (1998) Mathematical model of a adult human atrial cell. The role of K+ currents in repolarization. Circ Res 82:63–81
169. Nygren A, Leon LJ, Giles WR (2001) Simulations of the human atrial action potential. Philos Trans Roy Soc Lond 359:1111–1125
170. Oakes RS, Badger TJ, Kholmovski EG, Akoum N, Burgon NS, Fish EN, Blauer JJE, Rao SN, DiBella EVR, Segerson NM, Daccarett M, Windfelder J, McGann CJ, Parker D, MacLeod RS, Marrouche NF (2009) Detection and quantification of left atrial structural remodeling with delayed-enhancement magnetic resonance imaging in patients with atrial fibrillation. Circulation 119:1758–1767
171. van Oosterom A, Jacquemet V (2005) Genesis of the P wave: atrial signals as generated by the equivalent double layer source model. Europace 7 (Suppl 2):21–29
172. van Oosterom A, Jacquemet V (2009) Ensuring stability in models of atrial kinetics. In: Proceedings of computers in cardiology 2009, pp 69–72
173. Ordas S, Oubel E, Sebastian R, Frangi A (2007) Computational anatomy atlas of the heart. In: Proceedings of fifth international symposium of image and signal processing and analysis, pp 338–342
174. Otomo K, Uno K, Fujiwara H, Isobe M, Iesaka Y (2010) Local unipolar and bipolar electrogram criteria for evaluating the transmurality of atrial ablation lesions at different catheter orientations relative to the endocardial surface. Heart Rhythm 7:1291–1300
175. Papez JW (1920) Heart musculature of the atria. Am J Anat 27:255–286
176. Perez FJ, Wood MA, Schubert CM (2006) Effects of gap geometry on conduction through discontinuous radiofrequency lesions. Circulation 113:1723–1729
177. Plank G, Prassl A, Hofer E, Trayanova NA (2008) Evaluating intramural virtual electrodes in the myocardial wedge preparation: simulations of experimental conditions. Biophys J 94:1904–1915
178. Plank G, Prassl AJ, Wang JI, Seemann G, Scherr D, Sanchez-Quintana D, Calkins H, Trayanova NA (2008) Atrial fibrosis promotes the transistion of pulmonary vein ectopy into reentrant arrhythmias. Heart Rhythm
179. Platonov PG (2007) Interatrial conduction in the mechanisms of atrial fibrillation: from anatomy to cardiac signals and new treatment modalities. Europace 9 (Suppl 6):vi10–vi16
180. Platonov PG, Ivanov V, Ho SY, Mitrofanova L (2008) Left atrial posterior wall thickness in patients with and without atrial fibrillation: data from 298 consecutive autopsies. J Cardiovasc Electrophysiol 19:689–692
181. Ponto S, Schilling C, Krueger MW, Weber FM, Seemann S, Dössel O (2011) Influence of endocardial catheter contact on properties of the atrial signal and comparison with simulated electrograms. Biomed Tech 56(s1)
182. Pop M, Sermesant M, Peyratt JM, Crystal E, Dick AJ, Wright GA (2010) Anatomic reentry: Insights from a parametric study in a simple 3D anisotropic wedge model. Int J Bioelectromag 12:133–151

183. Pritchett AM, Jacobsen SJ, Mahoney DW, Rodeheffer RJ, Bailey KR, Redfield MM (2003) Left atrial volume as an index of left atrial size: a population-based study. J Am Coll Cardiol 41:1036–1043
184. Pullan AJ, Buist ML, Cheng LK (2005) Mathematically modelling the electrical activity of the heart: from cell to body surface and back again. World Scientific, Singapore
185. Qu Z, Weiss JN, Garfinkel A (2000) From local to global spatiotemporal chaos in a cardiac tissue model. Phys Rev E Stat Phys Plasmas Fluids Relat Interdiscip Topics 61:727–732
186. Ramirez RJ, Nattel S, Courtemanche M (2000) Mathematical analysis of canine atrial action potentials: rate regional factors and electrical remodeling. Am J Physiol Heart Circ Physiol 279:H1767–H1785
187. Ranjan R, Kato R, Zviman MM, Dickfeld TM, Roguin A, Berger RD, Tomaselli GF, Halperin HR (2011) Gaps in the ablation line as a potential cause of recovery from electrical isolation and their visualization using MRI. Circ Arrhythmia Electrophysiol
188. Reumann M, Bohnert J, Seemann G, Osswald B, Dössel O (2008) Preventive ablation strategies in a biophysical model of atrial fibrillation based on realistic anatomical data. IEEE Trans Biomed Eng 55:399–406
189. Richter U, Faes L, Cristoforetti A, Mase M, Ravelli F, Stridh M, Sornmo L (2011) A novel approach to propagation pattern analysis in intracardiac atrial fibrillation signals. Ann Biomed Eng 39:310–323
190. Ridler M, McQueen D, Peskin C, Vigmond E (2006) Action potential duration gradient protects the right atrium from fibrillating. In: Engineering in Medicine and Biology Society 2006. EMBS'06 28th annual international conference of the IEEE, pp 3978–3981
191. Ridler M.E, Lee M, McQueen D, Peskin C, Vigmond E (2011) Arrhythmogenic consequences of action potential duration gradients in the atria. Can J Cardiol 27:112–119
192. Rodriguez B, Burrage K, Gavaghan D, Grau V, Kohl P, Noble D (2010) The systems biology approach to drug development: application to toxicity assessment of cardiac drugs. Clin Pharmacol Therapeutics 88:130–134
193. Rogers JM, McCulloch AD (1994) A collocation-Galerkin finite element model of cardiac action potential propagation. IEEE Trans Biomed Eng 41:743–757
194. Rostock T, Steven D, Lutomsky B, Servatius H, Drewitz I, Klemm H, Mullerleile K, Ventura R, Meinertz T, Willems S (2008) Atrial fibrillation begets atrial fibrillation in the pulmonary veins: on the impact of atrial fibrillation on the electrophysiological properties of the pulmonary veins in humans. J Am Coll Cardiol 51:2153–2160
195. Rotter M, Dang L, Jacquemet V, Virag N, Kappenberger L, Haissaguerre M (2007) Impact of varying ablation patterns in a simulation model of persistent atrial fibrillation. Pacing Clin Electrophysiol 30:314–321
196. Ruchat P, Dang L, Schlaepfer J, Virag N, von Segesser LK, Kappenberger L (2007) Use of a biophysical model of atrial fibrillation in the interpretation of the outcome of surgical ablation procedures. Eur J Cardio Thorac Surg 32:90–95
197. Ruchat P, Dang L, Virag N, Schlaepfer J, von Segesser LK, Kappenberger L (2007) A biophysical model of atrial fibrillation to define the appropriate ablation pattern in modified maze. Eur J Cardio Thorac Surg 31:65–69
198. Ruiz-Villa CA, Tobon C, Rodriguez JF, Ferrero JM, Hornero F, Saiz J (2009) Influence of atrial dilatation in the generation of re-entries caused by ectopic activity in the left atrium. In: Proceedings of computers in cardiology. vol 36, pp 457–460
199. Correa de Sa DD, Thompson N, Stinnett-Donnelly J, Znojkiewicz P, Habel N, Muller JG, Bates JH, Buzas JS, Spector PS (2011) Electrogram fractionation: the relationship between spatio-temporal variation of tissue excitation and electrode spatial resolution. Circulation. Arrhythmia Electrophysiol 4(6):909–916
200. Sachse FB, Frech R, Werner CD, Dössel O (1999) A model based approach to assignment of myocardial fibre orientation. In: Proceedings of computers in cardiology. vol 26, pp 145–148, Hannover
201. Saffitz JE, Kanter HL, Green KG, Tolley TK, Beyer EC (1994) Tissue-specific determinants of anisotropic conduction velocity in canine atrial and ventricular myocardium. Circ Res 74:1065–1070
202. Saito T, Waki K, Becker A.E (2000) Left atrial myocardial extension onto pulmonary veins in humans: anatomic observations relevant for atrial arrhythmias. J Cardiovasc Electrophysiol 11:888–894
203. Sakamoto SI, Nitta T, Ishii Y, Miyagi Y, Ohmori H, Shimizu K (2005) Interatrial electrical connections: the precise location and preferential conduction. J Cardiovasc Electrophysiol 16:1077–1086
204. Sánchez C, Corrias A, Laguna P, Davies M, Swinton J, Jacobson I, Pueyo E, Rodriguez B (2010) Potential pharmacological therapies for atrial fibrillation. A computational study. In: Proceedings of computing in cardiology. vol 37, pp 413–416, IEEE 26–29 Sept 2010, Belfast
205. Sanchez-Quintana D, Anderson RH, Cabrera JA, Climent V, Martin R, Farre J, Ho SY (2002) The terminal crest: morphological features relevant to electrophysiology. Heart 88:406–411
206. Sanchez-Quintana D, Cabrera JA, Climent V, Anderson RH, Ho SY (2005) Sinus node revisited in the era of electroanatomical mapping and catheter ablation. Heart 91:189–194
207. Sanchez-Quintana D, Cabrera JA, Climent V, Farre J, Mendonca MCd, Ho SY (2005) Anatomic relations between the esophagus and left atrium and relevance for ablation of atrial fibrillation. Circulation 112:1400–1405
208. Saremi F, Channual S, Krishnan S, Gurudevan SV, Narula J, Abolhoda A (2008) Bachmann bundle and its arterial supply: imaging with multidetector CT–implications for interatrial conduction abnormalities and arrhythmias. Radiology 248:447–457
209. Saremi F, Krishnan S (2007) Cardiac conduction system: anatomic landmarks relevant to interventional electrophysiologic techniques demonstrated with 64-detector CT. Radiographics 27:1539–1565
210. Sassi R, Corino VDA, Mainardi LT (2009) Analysis of surface atrial signals: time series with missing data? Ann Biomed Eng 37:2082–2092
211. Sawa A, Shimizu A, Ueyama T, Yoshiga Y, Suzuki S, Sugi N, Oono M, Oomiya T, Matsuzaki M (2008) Activation patterns and conduction velocity in posterolateral right atrium during typical atrial flutter using an electroanatomic mapping system. Circ J 72:384–391
212. Schilling RJ, Peters NS, Goldberger J, Kadish AH, Davies DW (2001) Characterization of the anatomy and conduction velocities of the human right atrial flutter circuit determined by noncontact mapping. J Am Coll Cardiol 38:385–393
213. Schmitt C, Deisenhofer I, Zrenner B (eds) (2006) Catheter ablation of cardiac arrhythmias: a practical approach. Springer
214. Schotten U, Neuberger HR, Allessie MA (2003) The role of atrial dilatation in the domestication of atrial fibrillation. Prog Biophys Mol Biol 82:151–162
215. Schotten U, Verheule S, Kirchhof P, Goette A (2011) Pathophysiological mechanisms of atrial fibrillation: a translational appraisal. Physiol Rev 91:265–325
216. Schuster HP, Trappe HJ (2005) EKG-Kurs für Isabel. Georg Thieme Verlag, Stuttgart

217. Seemann G, Carillo P, Weiss DL, Krueger MW, Dössel O, Scholz EP (2009) Investigating arrhythmogenic effects of the hERG mutation N588K in virtual human atria. In: Ayache N, Delingette H, Sermesant M (eds) Lecture Notes in Computer Science, vol 5528, pp 144–153
218. Seemann G, Carrillo Bustamante P, Ponto S, Wilhelms M, Scholz EP, Dössel O (2010) Atrial fibrillation-based electrical remodeling in a computer model of the human atrium. In: Proceedings of computing in cardiology 37, pp 417–420
219. Seemann G, Höper C, Sachse FB, Dössel O, Holden AV, Zhang H (2006) Heterogeneous three-dimensional anatomical and electrophysiological model of human atria. Phil Trans Roy Soc A 364:1465–1481
220. Seemann G, Weiß DL, Sachse FB, Dössel O (2004) Familial atrial fibrillation: simulation of the mechanisms and effects of a slow rectifier potassium channel mutation in human atrial tissue. In: Proceedings of computers in cardiology. vol 31, pp 125–128
221. Severi S, Pogliani D, Fantini G, Fabbrini P, Viganò MR, Galbiati E, Bonforte G, Vincenti A, Stella A, Genovesi S (2010) Alterations of atrial electrophysiology induced by electrolyte variations: combined computational and P-wave analysis. Europace
222. Shah DC, Jais P, Haissaguerre M, Chouairi S, Takahashi A, Hocini M, Garrigue S, Clementy J (1997) Three-dimensional mapping of the common atrial flutter circuit in the right atrium. Circulation 96:3904–3912
223. Shenasa M, Hindricks G, Borggrefe M, Breithardt G (2009) Cardiac Mapping.
224. SippensGroenewegen A, Peeters HA, Jessurun ER, Linnenbank AC, Robles de Medina EO, Lesh MD, van Hemel NM (1998) Body surface mapping during pacing at multiple sites in the human atrium: P-wave morphology of ectopic right atrial activation. Circulation 97:369–380
225. Smaill BH, Hunter PJ (2010) Computer modeling of electrical activation: from cellular dynamics to the whole heart In: Cardiac electrophysiology methods and models, Springer, pp 159–185
226. Smith N, de Vecchi A, McCormick M, Camara O, Frangi AF, Delingette H, Sermesant M, Ayache N, Krueger MW, Schulze WHW, Hose R, Valverde I, Beerbaum P, Staicu C, Siebes M, Spaan J, Hunter P, Weese J, Lehmann H, Chapelle D, Rezavi R (2011) euHeart: personalized and integrated cardiac care using patient-specific cardiovascular modelling. J Roc Soc Interface
227. Spach M, Dolber PC, Heidlage JF (1988) Influence of the passive anisotropic properties on directional differences in propagation following modification of the sodium conductance in human atrial muscle: a model of reentry based on anisotropic discontinuous propagation. Circ Res 62:811–832
228. Stöllberger C, Ernst G, Bonner E, Finsterer J, Slany J (2003) Left atrial appendage morphology: Comparison of transesophageal images and postmortem casts. Springer Berlin / Heidelberg Zeitschrift für Kardiologie
229. Sunderman FW (1949) Anatomical normals. In: Normal values in clinical medicine. WB Saunders Co.
230. Syed Z, Vigmond E, Nattel S, Leon L (2005) Atrial cell action potential parameter fitting using genetic algorithms. Med Biol Eng Comput 43:561–571
231. Thomas SP, Wallace EM, Ross DL (2000) The effect of a residual isthmus of surviving tissue on conduction after linear ablation in atrial myocardium. J Interv Cardiac Electrophysiol 4:273–281
232. Tilg B, Fischer G, Modre R, Hanser F, Messnarz B, Schocke M, Kremser C, Berger T, Hintringer F, Roithinger FX (2002) Model-based imaging of cardiac electrical excitation in humans. IEEE Trans Med Imag 21:1031–1039
233. Tobón C, Ruiz C, Heidenreich E, Hornero F, Sáiz J (2009) Effect of the ectopic beats location on vulnerability to reentries in a three-dimensional realistic model of human atria. In: Proceedings of computers in cardiology. vol 36, pp 449–452
234. Tobón C, Ruiz C, Rodriguez JF, Hornero F, Ferrero JM, Saiz J (2010) A biophysical model of atrial fibrillation to simulate the Maze III ablation pattern. In:Proceedings of computers in cardiology. vol 37, pp 621–624
235. Tobón C, Ruiz C, Rodriguez JF, Hornero F, Ferrero JM, Saiz J (2010) Vulnerability for reentry in a three dimensional model of human atria: a simulation study. In: Engineering in medicine and biology society (EMBC) 2010 annual international conference of the IEEE, pp 224–227
236. Tobón C, Ruiz C, Sáiz J, Heidenreich E, Hornero F (2008) Reentrant mechanisms triggered by ectopic activity in a three-dimensional realistic model of human atrium. A computer simulation study. In: Proceedings of computers in cardiology. vol 35, pp 629–632
237. Tobón C, Sáiz J, Hornero F, Ruiz C, Hernándes V, Molto G (2006) Contribution of electrophysiological remodelling to generation of anatomical re-entries around the right pulmonary veins in human atrium: a simulation study. In: Proceedings of computers in cardiology. vol 33, pp 773–776
238. Toussaint N, Sermesant M, Stoeck C, Kozerke S, Batchelor P (2010) In vivo human 3D cardiac fibre architecture: reconstruction using curvilinear interpolation of diffusion tensor images. In: Proceedings of the 13th international conference on Medical image computing and computer-assisted intervention vol. 13, pp 418–425. Springer-Verlag
239. Trayanova NA (2011) Whole-heart modeling: applications to cardiac electrophysiology and electromechanics. Circ Res 108:113–128
240. Tsang TSM, Barnes ME, Gersh BJ, Bailey KR, Seward JB (2002) Left atrial volume as a morphophysiologic expression of left ventricular diastolic dysfunction and relation to cardiovascular risk burden. Am J Cardiol 90:1284–1289
241. Tsao HM, Yu WC, Cheng HC, Wu MH, Tai CT, Lin WS, Ding YA, Chang MS, Chen SA (2001) Pulmonary vein dilation in patients with atrial fibrillation: detection by magnetic resonance imaging. J Cardiovasc Electrophysiol 12:809–813
242. Tsujimae K, Murakami S, Kurachi Y (2008) In silico study on the effects of IKur block kinetics on prolongation of human action potential after atrial fibrillation-induced electrical remodeling. Am J Physiol Heart Circ Physiol 294:H793–H800
243. Uldry L, Jacquemet V, Virag N, Kappenberger L, Vesin JM (2012) Estimating the time scale and anatomical location of atrial fibrillation spontaneous termination in a biophysical model. Med Biol Eng Comput 50:155–163
244. Uldry L, Virag N, Jacquemet V, Vesin JM, Kappenberger L (2009) Spontaneous termination of atrial fibrillation: study of the effect of atrial geometry in a biophysical model. In: Engineering in medicine and biology society (EMBC) 2009 annual international conference of the IEEE, pp 4504–4507
245. Uldry L, Virag N, Jacquemet V, Vesin JM, Kappenberger L (2010) Optimizing local capture of atrial fibrillation by rapid pacing: study of the influence of tissue dynamics. Ann Biomed Eng 38:3664–3673
246. Uldry L, Virag N, Vesin JM, Kappenberger L (2010) Studies of therapeutic strategies for atrial fibrillation based on a biophysical model of the human atria patient-specific modeling of the cardiovascular system, Springer, New York pp 63–79.
247. Umapathy K, Masse S, Kolodziejska K, Veenhuyzen GD, Chauhan VS, Husain M, Farid T, Downar E, Sevaptsidis E, Nanthakumar K (2008) Electrogram fractionation in murine HL-1 atrial monolayer model. Heart Rhythm 5:1029–1035
248. Veinot JP, Lemery R (2005) Innovations in cardiovascular pathology: anatomic and electrophysiologic determinants

associated with ablation of atrial arrhythmias. Cardiovasc Pathol 14:204–213
249. Vigmond EJ, Ruckdeschel R, Trayanova N (2001) Reentry in a morphologically realistic atrial model. J Cardiovasc Electrophysiol 12:1046–1054
250. Vigmond EJ, Tsoi V, Yin Y, Page P, Vinet A (2009) Estimating atrial action potential duration from electrograms. IEEE Trans Biomed Eng 56:1546–1555
251. Virag N, Jacquemet V, Henriquez CS, Zozor S, Blanc O, Vesin JM, Pruvot E, Kappenberger L (2002) Study of atrial arrhythmias in a computer model based on magnetic resonance images of human atria. Chaos 12:754–763
252. Voigt I, Mansi T, Mihalef V, Ionasec R, Calleja, A, Mengue E, Sharma P, Houle H, Georgescu, B, Hornegger J, Comaniciu D (2011) LNCS (FIMH 2011) Lecture Notes in Computer Science, vol. 6666, chap. Patient-Specific Model of Left Heart Anatomy, Dynamics and Hemodynamics from 4D TEE: A First Validation Study, pp. 341–349. Springer Berlin/Heidelberg
253. Wang K, Ho SY, Gibson DG, Anderson RH (1995) Architecture of atrial musculature in humans. Br H J 73:559–565
254. Weber FM, Keller DUJ, Bauer S, Seemann G, Lorenz C, Dössel O (2011) Predicting tissue conductivity influences on body surface potentials: an efficient approach based on principal component analysis. IEEE Trans Biomed Eng 58:265–273
255. Weber FM, Luik A, Schilling C, Seemann G, Krueger MW, Lorenz C, Schmitt C, Dössel O (2011) Conduction velocity restitution of the human atrium: an efficient measurement protocol for clinical electrophysiological studies. IEEE Trans Biomed Eng 58:2648–2655
256. Weber FM, Schilling C, Seemann G, Luik A, Schmitt C, Lorenz C, Dössel O (2010) Wave-direction and conduction-velocity analysis from intracardiac electrograms: a single-shot technique. IEEE Trans Biomed Eng 57:2394–2401
257. Weber FM, Schilling C, Straub D, Gurm S, Seemann G, Lorenz C, Dössel O (2009) Extracting clinically relevant circular mapping and coronary sinus catheter potentials from atrial simulations. In: Lecture Notes in Computer Science, 5528, pp 30–38
258. Weese J, Peters J, Waechter I, Kneser R, Lehmann H, Ecabert O, Barschdorf H, Weber FM, Doessel O, Lorenz C (2010) The generation of patient-specific heart models for diagnosis and interventions. In: Lecture Notes in Computer Science 6364, pp 25–35
259. Werner CD, Sachse FB, Dössel O (2000) Electrical excitation propagation in the human heart. Int. J. Bioelectromagnetism 2
260. Wieser L, Fischer G, Hintringer F, Ho S, Tilg B (2005) Reentry anchoring at a pair of pulmonary vein ostia. In: Frangi A, Radeva P, Santos A, Hernandez M (eds) Functional imaging and modeling of the heart. Lecture Notes in Computer Science, vol 3504, Springer, Berlin, pp 183–194
261. Wieser L, Nowak CN, Tilg B, Fischer G (2008) Mother rotor anchoring in branching tissue with heterogeneous membrane properties. Biomed Eng 53:25–35
262. Wieser L, Richter HE, Plank G, Pfeifer B, Tilg B, Nowak CN, Fischer G (2008) A finite element formulation for atrial tissue monolayer. Method Inf Med 47:131–139
263. Wittkampf FHM, van Oosterhout MF, Loh P, Derksen R, Vonken Ej, Slootweg PJ, Ho SY (2005) Where to draw the mitral isthmus line in catheter ablation of atrial fibrillation: histological analysis. Eur Heart J 26:689–695
264. Young AA, Frangi AF (2009) Computational cardiac atlases: from patient to population and back. Exp Physiol 94:578–596
265. Yu WC, Lee SH, Tai CT (1999) Reversal of atrial electrical remodeling following cardioversion of long-standing atrial fibrillation in man. Cardiovasc Res 42:470–476
266. Zemlin CW, Herzel H, Ho SY, Panfilow A (2001) A realistic and efficient model of excitation propagation in the human atria Computer simulation and experimental assessment of cardiac electrophysiology. Futura, pp 29–34
267. Zhang H, Garratt CJ, Kharche S, Holden AV (2009) Remodelling of cellular excitation (reaction) and intercellular coupling (diffusion) by chronic atrial fibrillation represented by a reaction-diffusion system. Phys D Nonlin Phenom 238:976–983
268. Zhang H, Garratt CJ, Zhu J, Holden AV (2005) Role of up-regulation of IK1 in action potential shortening associated with atrial fibrillation in humans. Cardiovasc Res 66:493–502
269. Zhang H, Holden AV, Kodama I, Honjo H, Lei M, Varghese T, Boyett MR (2000) Mathematical models of action potentials in the periphery and center of the rabbit sinoatrial node. Am J Physiol Heart Circ Physiol 279:H397–H421
270. Zhang YH, Youm JB, Sung HK, Lee SH, Ryu SY, Ho WK, Earm YE (2000) Stretch-activated and background non-selective cation channels in rat atrial myocytes. J Physiol 523:607–619
271. Zhao J, Amiri A, Sands GB, Trew M, LeGrice, I, Smaill BH, Pullan AJ (2008) Structure specific models of electrical function in the right atrial appendage. In: Engineering in medicine and biology society (EMBC) 2008 Annual international conference of the IEEE, pp 145–148
272. Zhao J, Butters TD, Zhang H, Pullan AJ, LeGrice IJ, Sands GB, Smaill BH (2012) An image-based model of atrial muscular architecture: Effects of structural anisotropy on electrical activation. Circ Arrhythmia Electrophysiol (Epub ahead of print)
273. Zhao J, Trew ML, Legrice IJ, Smaill BH, Pullan AJ (2009) A tissue-specific model of reentry in the right atrial appendage. Journal of Cardiovascular Electrophysiology 20:675–684